J Biol Phys (2009) 35:383–411
DOI 10.1007/s10867-009-9155-y

ORIGINAL PAPER

Glutamate regulation of calcium and IP_3 oscillating and pulsating dynamics in astrocytes

Maurizio De Pittà · Mati Goldberg · Vladislav Volman · Hugues Berry · Eshel Ben-Jacob

Received: 3 February 2009 / Accepted: 14 April 2009 /
Published online: 12 June 2009

Abstract Recent years have witnessed an increasing interest in neuron–glia communication. This interest stems from the realization that glia participate in cognitive functions and information processing and are involved in many brain disorders and neurodegenerative diseases. An important process in neuron–glia communications is astrocyte encoding of synaptic information transfer—the modulation of intracellular calcium (Ca^{2+}) dynamics in astrocytes in response to synaptic activity. Here, we derive and investigate a concise mathematical model for glutamate-induced astrocytic intracellular Ca^{2+} dynamics that captures the essential biochemical features of the regulatory pathway of inositol 1,4,5-trisphosphate (IP_3). Starting from the well-known two-variable (intracellular Ca^{2+} and inactive IP_3 receptors) Li–Rinzel model for calcium-induced calcium release, we incorporate the regulation of IP_3 production and phosphorylation. Doing so, we extend it to a three-variable model (which we refer to as the *ChI* model) that could account for Ca^{2+} oscillations with endogenous IP_3 metabolism. This *ChI* model is then further extended into the G-*ChI* model to include regulation of IP_3 production by external glutamate signals. Compared with previous similar models, our three-variable models include a more realistic description of IP_3 production and degradation pathways, lumping together their

Electronic supplementary material The online version of this article (doi:10.1007/s10867-009-9155-y) contains supplementary material, which is available to authorized users.

M. De Pittà · M. Goldberg · E. Ben-Jacob (✉)
School of Physics and Astronomy, Tel Aviv University, 69978 Ramat Aviv, Israel
e-mail: eshel@tamar.tau.ac.il

V. Volman · E. Ben-Jacob
Center for Theoretical Biological Physics, UCSD, La Jolla, CA 92093-0319, USA

V. Volman
Computational Neurobiology Lab, The Salk Institute, La Jolla, CA 92037, USA

H. Berry
Project-Team Alchemy, INRIA Saclay, 91893 Orsay, France

essential nonlinearities within a concise formulation. Using bifurcation analysis and time simulations, we demonstrate the existence of new putative dynamical features. The cross-couplings between IP_3 and Ca^{2+} pathways endow the system with self-consistent oscillatory properties and favor mixed frequency–amplitude encoding modes over pure amplitude–modulation ones. These and additional results of our model are in general agreement with available experimental data and may have important implications for the role of astrocytes in the synaptic transfer of information.

Keywords Inositol 1,4,5-trisphosphate metabolism · Calcium signaling · Pulsating dynamics · Information encoding · Phase locking

1 Introduction

Astrocytes, the main type of glial cells in the brain, do not generate action potentials as neurons do, yet they can transfer information to other cells and encode information in response to external stimuli by employing "excitable"-like rich calcium (Ca^{2+}) dynamics [1]. Recognition of the potential importance of the intricate inter- and intracellular astrocyte dynamics has motivated, in recent years, intensive experimental efforts to investigate neuron–glia communication. Consequently, it was discovered that intracellular Ca^{2+} levels in astrocytes can be regulated by synaptic activity [2–6]. Responses to low-intensity synaptic stimulation or spontaneous astrocyte activity usually consist of spatially confined Ca^{2+} transients [3, 4, 7]. On the other hand, high-intensity synaptic activity or stimulation of adjacent sites within the same astrocytic process are generally associated with Ca^{2+} oscillations [8] that can bring forth propagation of both intracellular and intercellular waves [9–11]. Concomitantly, elevation of cytoplasmic Ca^{2+} induces the release from astrocytes of several neurotransmitters (or "gliotransmitters"), including glutamate, ATP, or adenosine (see Evanko et al. [12] for a review). These astrocyte-released gliotransmitters feed back onto pre- and postsynaptic terminals. This implies that astrocytes regulate synaptic information transfer [13–15]. Astrocytes can also mediate between neuronal activity and blood circulation [16], thus extending neuron–astrocyte communications to the level of neuronal metabolism [17].

The physiological meaning of astrocytic Ca^{2+} signaling remains currently unclear, and a long-standing question is how it participates in the encoding of synaptic information transfer [1, 18, 19]. Some of the available experimental data suggest a preferential frequency modulation (FM) mode of encoding, namely synaptic activity would be encoded in the frequency of astrocytic Ca^{2+} pulsations [20]. Indeed, cytoplasmic Ca^{2+} waves in astrocytes often appear as pulse-like propagating waveforms (namely pulses of width much smaller than their wavelength), whose frequency increases when the frequency or the intensity of synaptic stimulation grows [3].

Notwithstanding, the possibility of amplitude modulation (AM) encoding of synaptic activity or even of mixed amplitude and frequency modulation (AFM) encoding has also consistently been inferred [21]. For instance, the amplitude of Ca^{2+} oscillations in response to external stimuli can be highly variable, depending on the intensity of stimulation [2, 11, 22]. Experimental evidence suggests that Ca^{2+} dynamics does not simply mirror synaptic activity but is actually much more complex, to a point that astrocytes are suspected of genuine synaptic information processing [23]. The emerging picture is that the properties

of Ca^{2+} oscillations triggered by neuronal inputs in astrocytes (including their amplitude, frequency, and propagation) are likely to be governed by intrinsic properties of both neuronal inputs and astrocytes [1, 3].

From the modeling point of view, simplified or two-variable models for intracellular Ca^{2+} signaling can, in principle, be used to account for the diversity of the observed Ca^{2+} dynamics when the biophysical parameters are varied. We recently presented evidence that one of these two-variable models proposed by Li and Rinzel [24] actually predicts that the same cell could encode information about external stimuli by employing different encoding modes. In this model, changes of biophysical parameters of the cell can switch among AM of Ca^{2+} oscillations, FM of Ca^{2+} pulsations, or combined AM and FM (AFM) Ca^{2+} pulsations [18, 19]. We emphasize that one of the cardinal simplifications of the Li–Rinzel model is neglecting the regulation of inositol 1,4,5-trisphosphate (IP_3) dynamics, that is its production and degradation. Since IP_3 production is regulated by synaptic activity (via extracellular glutamate signaling), IP_3 dynamics has to be included for proper modeling of synapse–astrocyte communication. Only such modeling can provide a realistic account of astrocytic Ca^{2+} variations induced by nearby synaptic inputs.

Here, we introduce and investigate a concise model for glutamate-induced intracellular astrocytic dynamics. Using this model, we show new putative features of Ca^{2+} dynamics that can have important implications for the role of astrocytes in synaptic information transfer. Our model incorporates current biological knowledge related to the signaling pathways leading from extracellular glutamate to intracellular Ca^{2+}, via IP_3 regulation and IP_3-dependent Ca^{2+}-induced Ca^{2+} release (CICR). First, we extend the Li–Rinzel model to incorporate the regulation of IP_3. This yields a three-variable model, called hereafter the "*ChI*" model, for its state variables that are the intracellular Ca^{2+} level C, the fraction of inactive IP_3 receptors h, and the available IP_3 concentration I. Similar three-variable models have already been introduced in previous works [25–30] (see Falcke [31] for a review), yet our modeling includes a more realistic description of IP_3 dynamics, in particular with regard to the complex regulatory pathways of IP_3 formation and degradation. Furthermore, while we reduce these complex regulatory pathways to a concise mathematical description, we make sure to keep their essential nonlinearities. We then model the contribution of glutamate signals to IP_3 production and include this contribution as an additional production term into the IP_3 equation of the *ChI* model. We refer to this case as the "G-*ChI*" model.

We utilize bifurcation theory to study the coexistence of various encoding modes of synaptic activity by astrocytes: AM, pulsation FM, and mixed AFM. We also present results of time simulations of the model, illustrating the richness of intracellular Ca^{2+} dynamics (hence, of the encoding modes) in response to complex time-dependent glutamate signals.

We note that although the model presented here is derived for the specific case of astrocytes, our approach can be readily adopted to model Ca^{2+} dynamics in other cell types whose coordinated activity is based on intra- and intercellular Ca^{2+} signaling, such as heart cells, pancreas cells, and liver cells.

2 Derivation of the three-variable *ChI* model of intracellular Ca^{2+} dynamics

In this section, we describe the concise *ChI* model for intracellular Ca^{2+} dynamics in astrocytes with realistic IP_3 regulation. Given the relative intricacy of this signaling pathway (see Fig. 1), each basic building block of the model is described separately in the next sections.

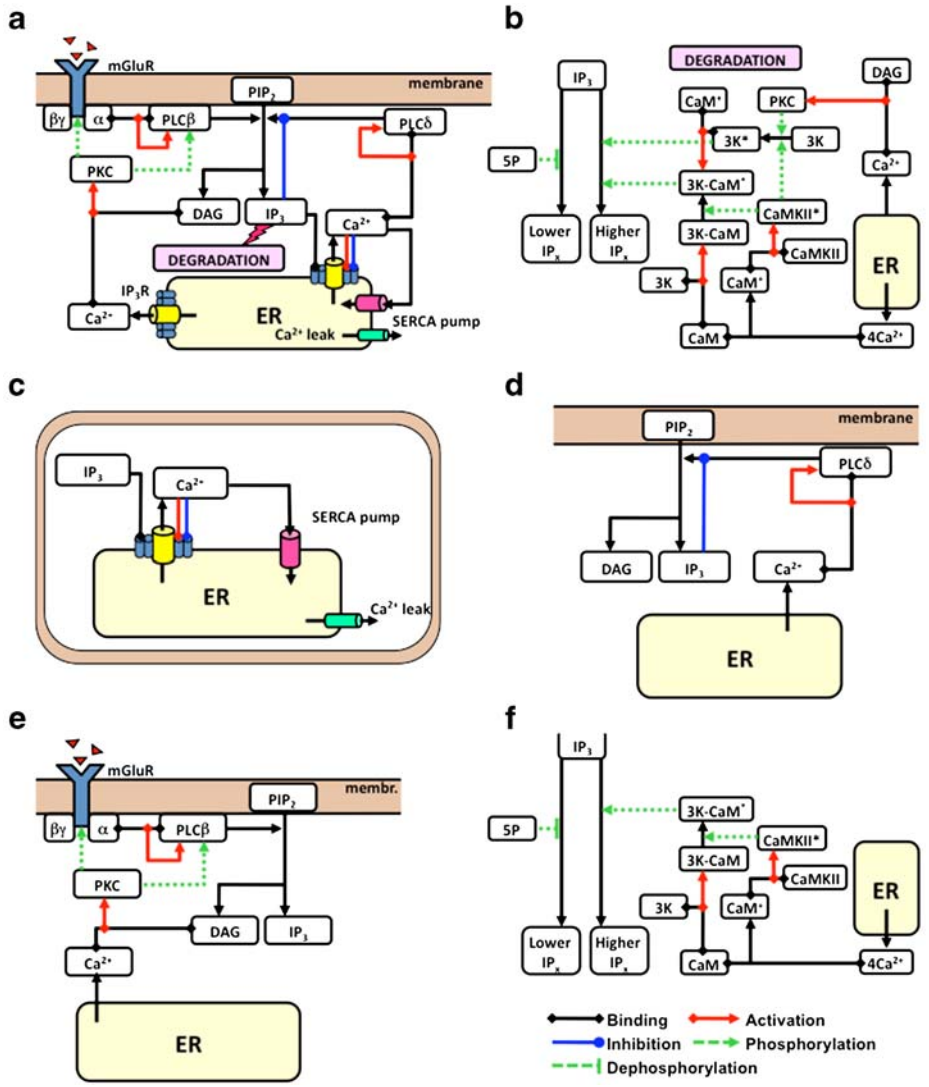

Fig. 1 Block diagrams of **a** production and **b** degradation of inositol 1,4,5-trisphosphate (IP_3), summarize the complexity of the signaling network underlying glutamate-induced intracellular dynamics of this second messenger. A peculiar feature of IP_3 metabolism is its coupling with intracellular calcium (Ca^{2+}) dynamics which, in astrocytes, primarily occurs through **c** Ca^{2+}-induced Ca^{2+} release from intracellular stores. Production of IP_3 is brought forth by hydrolysis of the highly phosphorylated membrane lipid phosphatidylinositol 4,5-bisphosphate (PIP_2) by PLCβ and PLCδ, two isoenzymes of the family of phosphoinositide-specific phospholipase C. **d** PLCδ signaling is agonist independent and modulated by Ca^{2+}. **e** The contribution of PLCβ to IP_3 production instead depends on agonist binding to G-protein coupled metabotropic receptors (mGluRs) found on the surface of the cell. Degradation of IP_3 mainly occurs through phosphorylation into inositol 1,3,4,5-tetrakisphosphate (IP_4), catalyzed by IP_3 3-kinase (3K), and dephosphorylation by inositol polyphosphate 5-phosphatase (5P). The activity of IP_3-3K is regulated by Ca^{2+} in a complex fashion which may be approximated as depicted in **f**. For simplicity, inhibition of IP-5P by Ca^{2+}/CaMKII-dependent phosphorylation [32] and competitive binding of IP_4 to IP-5P are not considered in this study. Legend of the different *arrows* is below **f**

2.1 CICR core and the two-variable Li–Rinzel model

Intracellular Ca^{2+} levels in astrocytes (as in most other cell types) can be modulated by several mechanisms. These include Ca^{2+} influx from the extracellular space or controlled release from intracellular Ca^{2+} stores such as the endoplasmic reticulum (ER) and mitochondria [33]. In astrocytes, though, IP_3-dependent CICR from the ER is considered the primary mechanism responsible of intracellular Ca^{2+} dynamics [34].

Calcium-induced Ca^{2+} release (see Fig. 1c) is essentially controlled by the interplay of two specific transports: efflux from the ER to the cytoplasm that is mediated by Ca^{2+}-dependent opening of the IP_3 receptor (IP_3R) channels and influx into the ER which is due to the action of sarco-endoplasmic reticulum Ca^{2+}-ATPase (SERCA) pumps. In basal conditions, however (when CICR is negligible), intracellular Ca^{2+} levels are set by the respective contributions of a passive Ca^{2+} leak from the ER, SERCA uptake, and plasma membrane Ca^{2+} transport [35, 36].

When synaptic activity is large enough, synaptically released glutamate may spill over the synaptic cleft and bind to the extracellular part of astrocytic metabotropic glutamate receptors (mGluRs) [4]. Binding of glutamate to mGluRs increases cytosolic IP_3 concentration and promotes the opening of a few IP_3R channels [37]. As a consequence, intracellular Ca^{2+} slightly increases. Since the opening probability of IP_3R channels nonlinearly increases with Ca^{2+} concentration [38], such an initial Ca^{2+} surge increases the opening probability of neighboring channels. In turn, this leads to a further increase of cytoplasmic Ca^{2+}. These elements therefore provide a self-amplifying release mechanism (hence the denomination of CICR). The autocatalytic action of Ca^{2+} release, however, reverses at high cytoplasmic Ca^{2+} concentrations, when inactivation of IP_3R channels takes place, leading to CICR termination [39]. In parallel, SERCA pumps, whose activity increases with cytoplasmic Ca^{2+} [40], quickly sequester excess cytoplasmic Ca^{2+} by pumping it back into the ER lumen. The intracellular Ca^{2+} concentration consequently recovers toward basal values which suppress IP_3R channel inactivation. Hence, if glutamatergic stimulation is prolonged, intracellular IP_3 remains high enough to repeat the cycle, and oscillations are observed [41].

The SERCA pump rate can be taken as an instantaneous function of cytoplasmic $[Ca^{2+}]$ (denoted hereafter by C) by assuming a Hill rate expression with exponent 2 (see Appendix 1):

$$J_{\text{pump}}(C) = v_{\text{ER}} \cdot \text{Hill}\left(C^2, K_{\text{ER}}\right) \tag{1}$$

where v_{ER} is the maximal rate of Ca^{2+} uptake by the pump and K_{ER} is the SERCA Ca^{2+} affinity, that is the Ca^{2+} concentration at which the pump operates at half of its maximal capacity [42].

The nonspecific Ca^{2+} leak current is assumed to be proportional to the Ca^{2+} gradient across the ER membrane by r_{L}, the maximal rate of Ca^{2+} leakage from the ER:

$$J_{\text{leak}}(C) = -r_{\text{L}}\left(C_{\text{ER}} - C\right) \tag{2}$$

where C_{ER} is the Ca^{2+} concentration inside the ER stores [36].

IP_3R channels can be thought of as ensembles of four independent subunits with three binding sites each: one for IP_3 and two for Ca^{2+}. The latter sites include an activation site and a separate site for inactivation [36]. IP_3-binding sensitizes the receptor toward activation by Ca^{2+} but only if both IP_3 and activating Ca^{2+}, are bound to a fixed set of three out of four subunits, the channel is open.

Assuming that the kinetic rates of the binding reactions are ordered such as IP_3-binding >> Ca^{2+}-activation >> Ca^{2+}-inactivation, Li and Rinzel proposed the following equation for the Ca^{2+} current through the IP_3R channels [24]:

$$J_{\text{chan}}(C, h, I) = r_C p^{\text{open}} (C_{\text{ER}} - C) \tag{3}$$

with the channel open probability given by $p^{\text{open}} = m_\infty^3 n_\infty^3 h^3$, where $m_\infty = \text{Hill}(I, d_1)$, $n_\infty = \text{Hill}(C, d_5)$, and h account for the three gating reactions, respectively, IP_3-binding, activating Ca^{2+}-binding, and Ca^{2+}-dependent inactivation of the receptor. The power of 3 was directly suggested by experimental data [36, 38]. Finally, I stands for the intracellular IP_3 concentration and r_C is the maximum channel permeability.

Since Ca^{2+} fluxes across the plasma membrane have been proven not necessary for the onset of CICR [35, 43, 44], they can be neglected, so that the cell-averaged total free Ca^{2+} concentration (C_0) is conserved. Hence, the ER Ca^{2+} concentration (C_{ER}) can be rewritten in terms of equivalent cell parameters as $C_{\text{ER}} = (C_0 - C)/c_1$ where c_1 is the ratio between the ER and the cytosol volumes. It follows that J_{chan} and J_{leak} can entirely be expressed as functions of cell parameters, namely:

$$\begin{aligned} J_{\text{chan}} &= r_C m_\infty^3 n_\infty^3 h^3 (C_0 - (1 + c_1) C) \\ J_{\text{leak}} &= r_L (C_0 - (1 + c_1) C). \end{aligned} \tag{4}$$

Adding together the above terms (1) and (4), the cytoplasmic Ca^{2+} balance is given by:

$$\dot{C} = \left(r_C m_\infty^3 n_\infty^3 h^3 + r_L\right)(C_0 - (1 + c_1) C) - v_{\text{ER}} \frac{C^2}{C^2 + K_{\text{ER}}^2}. \tag{5}$$

This equation is coupled with an equation for h that accounts for the kinetics of IP_3Rs [24]:

$$\dot{h} = \frac{h_\infty - h}{\tau_h}, \tag{6}$$

where:

$$h_\infty = \frac{Q_2}{Q_2 + C}, \quad \tau_h = \frac{1}{a_2 (Q_2 + C)}, \quad \text{and} \quad Q_2 = d_2 \frac{I + d_1}{I + d_3}.$$

Equations 5 and 6 form the so-called Li–Rinzel (L–R) model of CICR and constitute the core mechanism of our model for astrocyte Ca^{2+} signaling. We discuss below some of its properties.

2.2 AM, FM, and AFM encoding modes in the Li–Rinzel model

Calcium acts as a second messenger and transmits information from the extracellular side of the plasma membrane to targets within the cell [33, 45, 46]. In the case of Ca^{2+} signaling in astrocytes, however, the information usually arrives as a nonoscillatory stimulus at the plasma membrane and is translated into intracellular Ca^{2+} oscillations. For instance, glutamate concentration at the extracellular side of the astrocyte membrane determines the degree of activation of mGluRs and therefore can be directly linked to intracellular IP_3 concentration [47]. It follows that in the L–R model, the level of IP_3 can be thought as being directly controlled by glutamate signals impinging on the cell from its external environment. In turn, the level of IP_3 determines the dynamics of intracellular Ca^{2+}. In

physiological conditions glutamate-induced astrocyte Ca^{2+} signaling is synaptically evoked [2–4]. One can therefore think of the Ca^{2+} signal as being an encoding of information about the level of synaptically released glutamate and ultimately of synaptic activity. Notably, this information encoding can use AM, FM, or both modulations (AFM) of Ca^{2+} oscillations and pulsations.

We have recently shown that these encoding modes may actually depend on inherent cellular properties [18, 19]. In particular, the stronger the SERCA uptake with respect to Ca^{2+} efflux from the ER, the more pulsating and FM-like the encoding. A fast uptake by SERCAs, in fact, firmly counteracts CICR, so that higher Ca^{2+} levels are required for the onset of this latter one. When this happens, however the effects of CICR are large and the increase of intracellular Ca^{2+} is fast and remarkable. Accordingly, inactivation of IP_3R channels is also faster and basal Ca^{2+} levels are recovered rapidly. In these conditions, the IP_3 level modulates the onset of CICR (through m_∞) thus setting the frequency of pulsation (FM encoding). On the contrary, the AM case is observed with weaker Ca^{2+} uptake by SERCAs. Weaker SERCA rates in fact allow for smoother oscillations whose amplitude is mainly dependent on the interplay between CICR onset and Ca^{2+}-dependent inactivation. Hence, the amplitude of oscillations in these latter conditions depends on IP_3, whereas their frequency does not, as it is essentially fixed by IP_3R channel recovery from Ca^{2+}-dependent inactivation [19].

From a dynamical systems perspective, AM and FM encoding are associated with well-distinct bifurcation diagrams. Amplitude modulations of Ca^{2+} oscillations are typically found when the system exhibits Hopf bifurcations only. In particular, when oscillations are born through a supercritical Hopf bifurcation at low IP_3 concentration, then AM encoding exists (Fig. 2a–c). Alternatively, if the Hopf bifurcation is subcritical, AFM might be found [18]. On the contrary, in FM (Fig. 2d–f), the presence of a saddle-node homoclinic bifurcation accounts for pulsatile oscillations which arise at arbitrarily small frequency but with amplitude essentially independent of the IP_3 value [19].

Finally, it is important to note that the L–R model assumes that IP_3 does not vary with time nor depends on the other variables (that is, its concentration I, in (5) and (6), is a parameter of the model). Yet examination of the underlying signaling pathways (Fig. 1) immediately hints that IP_3 concentration indeed depends on both intracellular Ca^{2+} and extracellular glutamate, so that IP_3 should be an additional variable in the model. Our aim in the present article is to devise a model that incorporates these dependencies.

2.3 IP_3 regulation: the *ChI* model

2.3.1 PLCδ production

In astrocytes, IP_3 together with diacylglycerol (DAG) is produced by hydrolysis of phosphatidylinositol 4,5-bisphosphate (PIP_2) by two phosphoinositide-specific phospholipase C (PLC) isoenzymes, PLCβ and PLCδ [48]. The activation properties of these two isoenzymes are different and so, it is likely, are their roles. PLCβ is primarily controlled by cell surface receptors; hence, its activity is linked to the level of external stimulation (i.e., the extracellular glutamate) and as such, it pertains to the glutamate-dependent IP_3 metabolism and will be addressed in the next section.

On the contrary, PLCδ is essentially activated by increased intracellular Ca^{2+} levels (Fig. 1d) [49]. Structural and mutational studies of complexes of PLCδ with Ca^{2+} and IP_3 revealed complex interactions of Ca^{2+} with several negatively charged residues within its catalytic domain [50–52], a hint of cooperative binding of Ca^{2+} to this enzyme. In

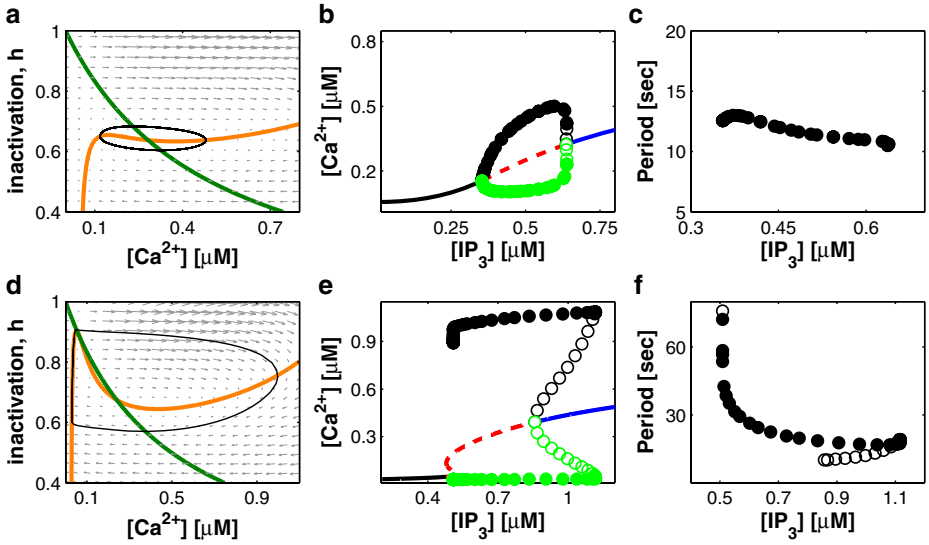

Fig. 2 Both AM-encoding or FM-encoding Ca^{2+} oscillations can be generated by the Li–Rinzel model for CICR, depending on the value of K_{ER}, the Ca^{2+} affinity of sarco-endoplasmic reticulum Ca^{2+}-ATPase pumps. For example, AM encoding can be found at **a**–**c** $K_{ER} = 0.1$ μM whereas FM encoding exists for smaller K_{ER}, such as **d**–**f** $K_{ER} = 0.05$ μM. **a** In the phase plane, AM encoding is associated with a single intersection between the *C*-nullcline (*orange*) and the *h*-nullcline (*green*). These are the curves for which $\dot{C} = 0$ and $\dot{h} = 0$, respectively. Accordingly, the only possible bifurcations that can be found are connected with loss/gain of stability, i.e., they are Hopf bifurcations. **b** The associated bifurcation diagram indeed shows that oscillations arise via supercritical Hopf bifurcation (H_1) at $[Ca^{2+}] \approx 0.15$ μM and $[IP_3] \approx 0.36$ μM, whereas they die at $[Ca^{2+}] \approx 0.32$ μM and $[IP_3] \approx 0.64$ μM via a subcritical Hopf bifurcation (H_2). The fact that H_1 is supercritical accounts for the occurrence of oscillations of arbitrarily small amplitude that increases with IP_3 yet with almost constant period (**c**). **d** In FM-encoding conditions, the *C*-nullcline is sharply *N*-shaped and there exists a small range of IP_3 values where it can intersect the *h*-nullcline at three points. **e** This region is delimited by two "knees" shown by the fixed-point continuation curve, which correspond to a saddle-node bifurcation at $[Ca^{2+}] \approx 0.13$ μM and $[IP_3] \approx 0.48$ μM and a saddle-node homoclinic bifurcation at $[Ca^{2+}] \approx 0.07$ μM and $[IP_3] \approx 0.53$ μM. Pulsatile oscillations arise and die via subcritical Hopf bifurcations respectively at H_1 ($[Ca^{2+}] \approx 0.05$ μM, $[IP_3] \approx 0.51$ μM) and H_2 ($[Ca^{2+}] \approx 0.39$ μM, $[IP_3] \approx 0.86$ μM). While their amplitude is essentially constant, their period can be arbitrarily long (**f**) due to the saddle-node homoclinic bifurcation. **b**, **e** Conventions: stable equilibria are shown as *solid lines*, respectively for low (*black*) and high (*blue*) IP_3 concentrations. Unstable equilibria are displayed as *red dashed lines*. Oscillations are located in the diagram as min (*green*)–max (*black*) envelopes, with stable oscillations as *filled circles* and unstable ones as *empty circles*. Parameter values for the L–R model as in Table 1

agreement with these experimental findings, the PLCδ activation rate can be written as [27, 53]:

$$v_\delta(C, I) = v'_\delta(I) \cdot \text{Hill}\left(C^2, K_{\text{PLC}\delta}\right) \tag{7}$$

where the maximal rate of activation depends on the level of intracellular IP_3. Experimental observations show that high (>1 μM) IP_3 concentrations inhibit PLCδ activity by competing with PIP_2 binding to the enzyme [54]. Accordingly, assuming competitive binding [55], the maximal PLCδ-dependent IP_3 production rate can be modeled as follows:

$$v'_\delta(I) = \frac{\bar{v}_\delta}{1 + \frac{I}{\kappa_\delta}} \tag{8}$$

where κ_δ is the inhibition constant of PLCδ activity.

Table 1 Parameter values for the *ChI* and G-*ChI* models

Parameter	Unit	Description	AM	FM
		L–R core [18, 24]		
r_C	s^{-1}	Maximal CICR rate	6	
r_L	s^{-1}	Maximal rate of Ca^{2+} leak from the ER	0.11	
C_0	μM	Total cell free Ca^{2+} concentration referred to the cytosol volume	2	
c_1	–	Ratio between cytosol volume and ER volume	0.185	
v_{ER}	μM s^{-1}	Maximal rate of SERCA uptake	0.9	
K_{ER}	μM	SERCA Ca^{2+} affinity	0.1	0.05
d_1	μM	IP_3 dissociation constant	0.13	
d_2	μM	Ca^{2+} inactivation dissociation constant	1.049	
d_3	μM	IP_3 dissociation constant	0.9434	
d_5	μM	Ca^{2+} activation dissociation constant	0.08234	
a_2	s^{-1}	IP_3R binding rate for Ca^{2+} inhibition	0.2	
		Agonist-independent IP_3 production [27, 48, 53]		
$\bar{v}_\delta$	μM s^{-1}	Maximal rate of IP_3 production by PLCδ	0.02	0.05
$K_{PLC\delta}$	μM	Ca^{2+} affinity of PLCδ	0.1	
κ_δ	μM	Inhibition constant of PLCδ activity	1.5	
		IP_3 degradation [56–59]		
$\bar{r}_{5P}$	s^{-1}	Maximal rate of degradation by IP-5P	0.04	0.05
$\bar{v}_{3K}$	μM s^{-1}	Maximal rate of degradation by IP_3-3K	2	
K_D	μM	Ca^{2+} affinity of IP_3-3K	0.7	
K_3	μM	IP_3 affinity of IP_3-3K	1	
		Agonist-dependent IP_3 production [27, 60–62]		
$\bar{v}_\beta$	μM s^{-1}	Maximal rate of IP_3 production by PLCβ	0.2	0.5
K_R	μM	Glutamate affinity of the receptor	1.3	
K_p	μM	Ca^{2+}/PKC-dependent inhibition factor	10	
K_π	μM	Ca^{2+} affinity of PKC	0.6	

Figure 3 shows the behavior of this term when Ca^{2+} and corresponding IP_3 levels obtained from the bifurcation diagrams of the L–R model in Fig. 2 are substituted into (7). We have set $K_{PLC\delta}$ to a value that is close to the Ca^{2+} concentration of the lower bifurcation point. This allows us to translate the large-amplitude Ca^{2+} oscillations into oscillations of v_δ that could preserve the main AM/FM properties.

2.3.2 IP_3 degradation

Two major IP_3 degradation pathways have been described so far (Fig. 1b). The first one is through dephosphorylation of IP_3 by inositol polyphosphate 5-phosphatase (IP-5P). The other one occurs through phosphorylation of IP_3 by the IP_3 3-kinase (IP_3-3K) and is Ca^{2+} dependent [63].

The rate of both IP-5P dephosphorylation (v_{5P}) and IP_3-3K phosphorylation (v_{3K}) of IP_3 can be considered as of Michaelis–Menten type [56, 64, 65]. Therefore:

$$\begin{aligned} v_{5P}(I) &= \bar{v}_{5P} \cdot \mathrm{Hill}(I, K_5) \\ v_{3K}(C, I) &= v^*_{3K}(C) \cdot \mathrm{Hill}(I, K_3). \end{aligned} \tag{9}$$

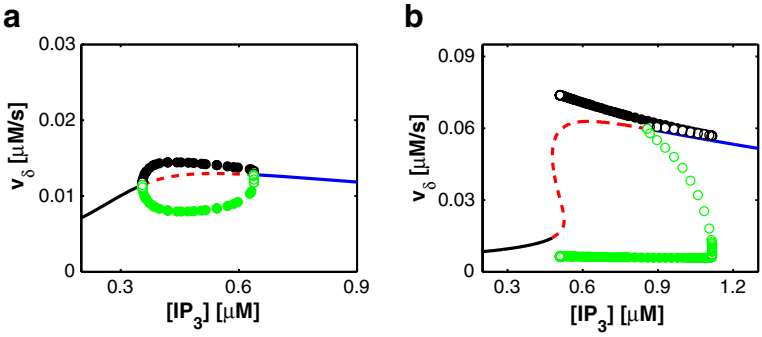

Fig. 3 Bifurcation diagrams for PLCδ-dependent IP_3 production are drawn by substituting into (7), $[Ca^{2+}]$ and $[IP_3]$ values obtained from the bifurcation diagrams in Fig. 2b (panel **a** above) and in 2e (panel **b** above), respectively. *Colors* as in Fig. 2b, e

Since $K_5 > 10$ μM [57, 66] and physiological levels of IP_3 are in general below this value, IP-5P is likely not to be saturated by IP_3. It follows that the rate of IP_3 degradation by IP-5P can be linearly approximated:

$$\nu_{5P}(I) \approx \bar{r}_{5P} \cdot I \tag{10}$$

where $\bar{r}_{5P}$ is the linear rate of IP_3 degradation by IP-5P and can be defined by parameters in (9) as $\bar{r}_{5P} = \bar{v}_{5P}/K_5$.

In basal conditions, phosphorylation of IP_3 by IP_3-3K is very slow. The activity of IP_3-3K is substantially stimulated by Ca^{2+}/calmodulin (CaM) via CaMKII-catalyzed phosphorylation (Fig. 1b) [67]. However, other experimental reports have suggested that Ca^{2+}-dependent PKC phosphorylation of IP_3-3K could have inhibitory effects [68]. Notwithstanding, evidences for this latter possibility are contradictory [69]. Hence, for the sake of simplicity, we have chosen in the present model to consider the simplified case where only CaMKII-catalyzed phosphorylation of IP_3-3K is present (Fig. 1f).

Phosphorylation of IP_3-3K by active CaMKII (CaMKII*) only occurs at a single threonine residue [67, 70], therefore we can assume that $v^*_{3K}(C) \propto$ [CaMKII*]. Activation of CaMKII is Ca^{2+}/CaM dependent and occurs in a complex fashion because of the unique structure of this kinase which is composed of ∼12 subunits with three to four phosphorylation sites each [71]. Briefly, Ca^{2+} elevation leads to the formation of a Ca^{2+}–CaM complex (CaM^+) that may induce phosphorylation of some of the sites of each CaMKII subunit. CaMKII quickly and fully activates when two of these sites (at proximal subunits) are phosphorylated [72]. In spite of the occurrence of multiple CaM^+ binding to the inactive kinase, experimental investigations showed that KII activation by CaM^+ can be approximated by a Hill equation with unitary coefficient [58]. Hence, if we surmise the following kinetic reaction scheme for CaMKII phosphorylation:

$$\begin{aligned} 4Ca^{2+} + CaM &\underset{k_u}{\overset{k_b}{\rightleftarrows}} CaM^+ \\ KII + CaM^+ &\underset{k_{-1}}{\overset{k_1}{\rightleftarrows}} CaMKII \underset{k_{-2}}{\overset{k_2}{\rightleftarrows}} CaMKII^*, \end{aligned} \tag{11}$$

it can be demonstrated that [CaMKII*] ∝ Hill(C^4, K_D) (see Appendix 2).

Accordingly, $v^*_{3K}(C) \propto \text{Hill}\left(C^4,\ K_D\right)$ and the equation for IP_3-3K-dependent IP_3 degradation reads:

$$v_{3K}(C, I) = \bar{v}_{3K} \cdot \text{Hill}\left(C^4, K_D\right) \cdot \text{Hill}(I, K_3)\,. \tag{12}$$

Experimental observations show the existence of three regimes of IP_3 metabolism [57]. At low $[Ca^{2+}]$ and $[IP_3]$ (<400 nM and <1 μM, respectively), IP-5P and IP_3-3K degrade roughly the same amounts of IP_3. Then, at high $[Ca^{2+}]$ (≥400 nM) but low $[IP_3]$ (≤8 μM), IP_3 is predominantly metabolized by IP_3-3K. Eventually, for $[IP_3]$ greater than 8 μM, when IP_3-3K activity saturates, IP-5P becomes the dominant metabolic enzyme, independently of $[Ca^{2+}]$.

In our modeling, the third regime—corresponding to $[IP_3] > 8$ μM—exceeds the range of validity for the linear approximation of IP-5P degradation (10) and therefore cannot be taken into account. However, it can be shown that the first two regimes are sufficient to reproduce Ca^{2+} oscillations and pulsations, thus restricting the core features of IP_3 metabolism to the maximal rates of IP_3 degradation by IP_3-3K and IP-5P and to the Ca^{2+} dependence of IP_3-3K. In particular, by opportune choice of parameters such as $\bar{v}_{3K} > K_3 \bar{r}_{5P}$, theoretical investigations showed that these two regimes are essentially generated by the Ca^{2+}-dependent Hill term in the expression of v_{3K} irrespectively of the assumption of Michaelis–Menten kinetics for IP_3 dependence of IP_3-3K (Fig. 4). Accordingly, a linear approximation for v_{3K} such as:

$$v_{3K}(C, I) = \bar{r}_{3K} \cdot \text{Hill}\left(C^4, K_D\right) \cdot I \tag{13}$$

where $\bar{r}_{3K} = \bar{v}_{3K}/K_3$ could also be considered instead of (12), in agreement with previous investigations found in the literature [26, 57].

Indeed, the behaviors of v_{3K} in (12) and (13) for IP_3 and Ca^{2+} concentrations obtained from the corresponding Li–Rinzel bifurcation diagrams are qualitatively similar (Fig. 5). Moreover, the overall bifurcation diagrams are largely conserved (results not shown). The

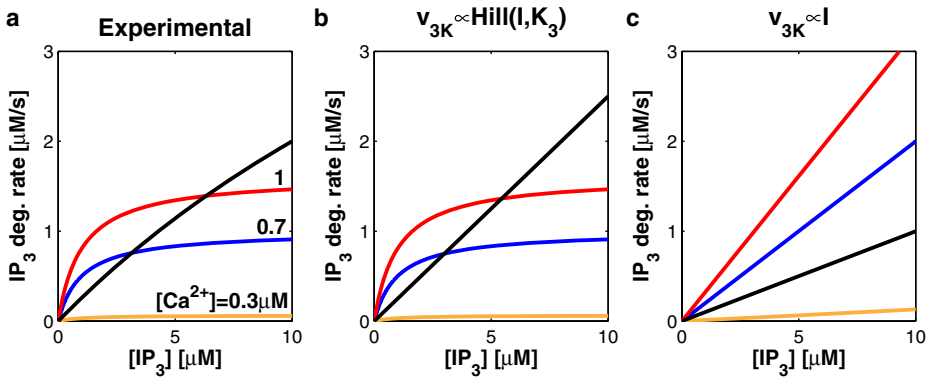

Fig. 4 **a** Experimental observations suggest the existence of three regimes of IP_3 metabolism: one for low $[Ca^{2+}]$ and $[IP_3]$ in which IP_3-3K (Ca^{2+}-dependent *color* curves) and IP-5P (*black* curve) activities are similar; an intermediate one for higher $[Ca^{2+}]$ in which IP_3 degradation by IP_3-3K is predominant; and a third one for $[IP_3] > 8$ μM in which IP_3 is degraded mainly by IP-5P in a Ca^{2+}-independent fashion. Both enzymes can be assumed Michaelis–Menten. **b**, **c** Physiological IP_3 concentrations suggest only the first two regimes. Notably, these latter regimes can be mimicked either **b** by keeping the hypothesis of Michaelis–Menten kinetics for IP_3-3K (9) or **c** by a linear approximation of this dependence (13)

main quantitative difference is that the linear approximation yields stronger degradation rates. In particular, the IP_3-3K rate can be up to twofold higher in (13) than in (12). This is particularly marked when high $[Ca^{2+}]$ is reached, such as in FM conditions (Fig. 5c–d). Notwithstanding, the Michaelis–Menten constant of IP_3-3K for its substrate is experimentally reported to be $K_3 \approx 1$ μM [56, 59] and it is likely that intracellular IP_3 levels can reach such micromolar concentrations in vivo [73]. Therefore, in the following, we will keep the Michaelis–Menten formulation for v_{3K} (12).

Finally, experimental measurements show that for $[Ca^{2+}] > 1$ μM and low IP_3 levels, the IP_3-3K activity exceeds that of IP-5P by almost 20-fold. In the model, this means that if $I << K_3$ (i.e., $v_{3K}(C, I) \approx \bar{r}_{3K} \times I$), then $v_{3K} \approx 20 v_{5P}$. Accordingly, we set the maximal degradation rates in the following such that $\bar{v}_{3K} \approx 20 K_3 \bar{r}_{5P}$.

2.3.3 Model analysis

In summary, our model of Ca^{2+} dynamics with endogenous IP_3 metabolism is based on the two L–R equations ((5) and (6)), but the IP_3 concentration (I) is now provided by a third coupled differential equation (summing the terms given by (7), (10), (12)):

$$\dot{I} = \frac{\bar{v}_\delta}{1 + \frac{I}{\kappa_\delta}} \mathrm{Hill}\left(C^2, K_{\mathrm{PLC}\delta}\right) - v_{3K} \mathrm{Hill}\left(C^4, K_D\right) \mathrm{Hill}\left(I, K_3\right) - r_{5P} I. \tag{14}$$

Equation 14 together with (5) and (6) define our three-variable "*ChI*" model, whose name is composed of the letters denoting its state variables.

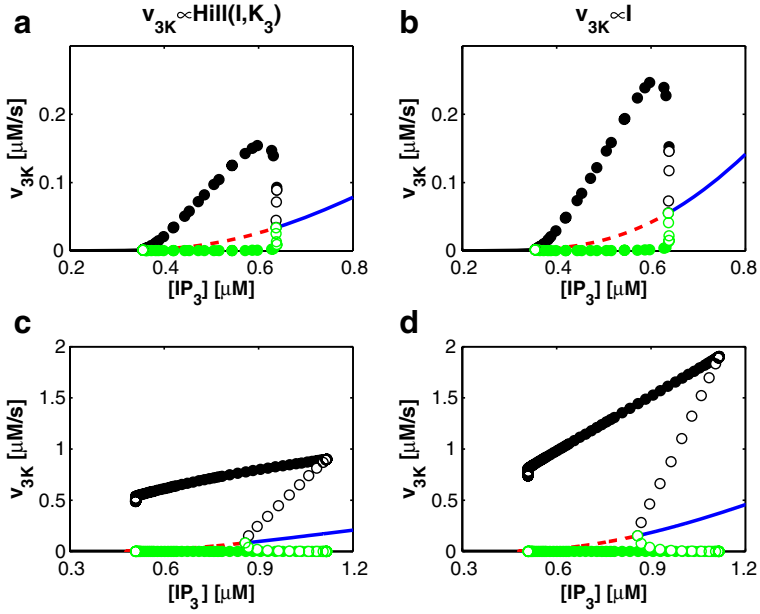

Fig. 5 Bifurcation behaviors of IP_3-3K-dependent IP_3 degradation in **a**, **b** AM and **c**, **d** FM conditions are compared for **a**, **c** Michaelis–Menten (12) or **b**, **d** linear approximations (13) of the IP_3 dependence of IP_3-3K rate. Despite qualitatively similar behaviors, the linear approximation is not further taken into account in the present study, because IP_3-3K activity may saturate in physiological conditions, thus invalidating the linear approximation

Consistency of the *ChI* model with respect to the L–R core model was sought by comparing two curves for pseudosteady states. First, we set $\dot{I} = 0$ and $C \to 0$ in (14) and solved for I as a function of C in the resulting equation. In parallel, we set $\dot{C} = 0$ in (5) and solved for I as a function of C in the resulting equation as well. The two resulting I–C curves should be as similar as possible. Analysis showed that they are indeed relatively similar (Fig. 6) if one chooses $K_{PLC\delta} \leq H_1$, $K_D \approx H_2$, $K_3 > H_2$, where H_1 and H_2 denote Ca^{2+} and IP_3 concentrations at the two Hopf bifurcations in the L–R bifurcation diagrams (Fig. 2). Such choice of parameters together with the others given in Table 1 ensures the existence of Ca^{2+} and IP_3 oscillations with amplitudes that are in agreement with those reported in the literature ([73];see Fig. 3 of Online Supplementary Material).

An important feature of our model is that despite the coupling between Ca^{2+} and IP_3, the equation for Ca^{2+} dynamics (5) does not contain parameters found within the equation for IP_3 dynamics (14). This means that the equation of the C-nullcline does not change with respect to the L–R model. Because the shape of this nullcline is crucial for the encoding mode (see Fig. 2a, c), the occurrence of AM, FM, or AFM modes in the *ChI* model is essentially established by the parameters of the L–R core model.

The only possible way that IP_3 metabolism could affect the encoding mode is by modulating the dynamics of the channel inactivation variable h. This mechanism is suggested by the projection of the surfaces for $\dot{C} = 0$, $\dot{h} = 0$, and $\dot{I} = 0$ (Fig. 7) onto the C–I plane for different values of h and C (Fig. 8). We note indeed that the C-nullcline depends on the value of h but not the I-nullcline. In contrast, both the h-nullcline and the I-nullcline change with C, which suggests that the coupling between Ca^{2+} and IP_3 dynamics essentially occurs through h. We may expect that, since h sets the slow time scale of the oscillations, the effect of IP_3 metabolism on Ca^{2+} dynamics in our model is mainly a modulation of the oscillation frequency. This aspect is further discussed in Sections 4 and 5, following the introduction in the next section of the last term of our model, namely the glutamate-dependent IP_3 production.

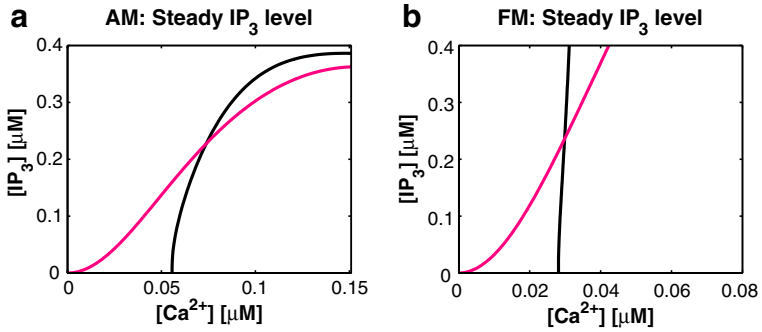

Fig. 6 Consistency of the equation for the endogenous IP_3 metabolism with respect to the L–R core model can be tested as follows: at resting physiological conditions: $\dot{C} = \dot{I} = 0$, $h = h_\infty(C)$ and $C \to 0$ so that $v_{3K}(C, I_s) \approx 0$. Hence, for steady IP_3 values (I_s) such as $I_s << \kappa_\delta$, one gets $v_\delta(C, I_s) \approx \bar{v}_\delta \cdot \mathrm{Hill}\left(C^2, K_{PLC\delta}\right)$. Accordingly, (14) can be solved for I_s, yielding $I_s(C) \approx r_{5P}^{-1} \cdot \bar{v}_\delta \cdot \mathrm{Hill}\left(C^2, K_{PLC\delta}\right)$ (*magenta* curve). The latter curve must be compared with the corresponding $I(C)$ curve (*black*) obtained by solving for I the equation $\dot{C}|_{h=h_\infty(C)} = 0$ in the original L–R model (5). By changing $\bar{v}_\delta$, $\bar{r}_{5P}$, $K_{PLC\delta}$, and κ_δ according to their experimental values, we seek consistency when $I_s(C) \approx I(C)$. In these conditions, in fact, our mathematical description of IP_3 metabolism and the L–R model predict equivalent steady intracellular IP_3 levels

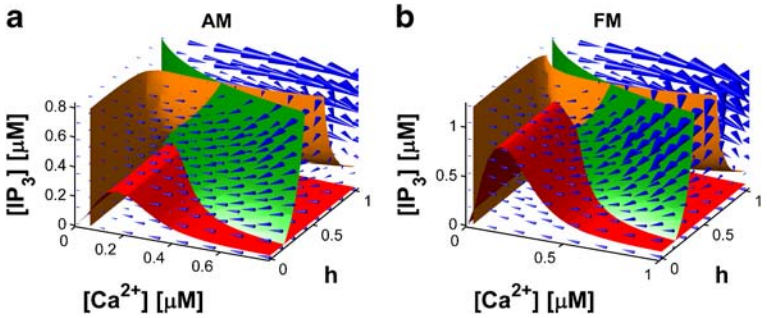

Fig. 7 Surfaces for $\dot{C} = 0$ (*orange*), $\dot{h} = 0$ (*green*), and $\dot{I} = 0$ (*red*) for the *ChI* model described by (5), (6), and (14)

3 Modeling glutamate regulation of IP_3 production: the G-*ChI* model

The contribution of glutamate signals to IP_3 production can be taken into account as an additional production term in the IP_3 equation of the above three-variable *ChI* model. The resulting new model is referred to as the "G-*ChI*" model.

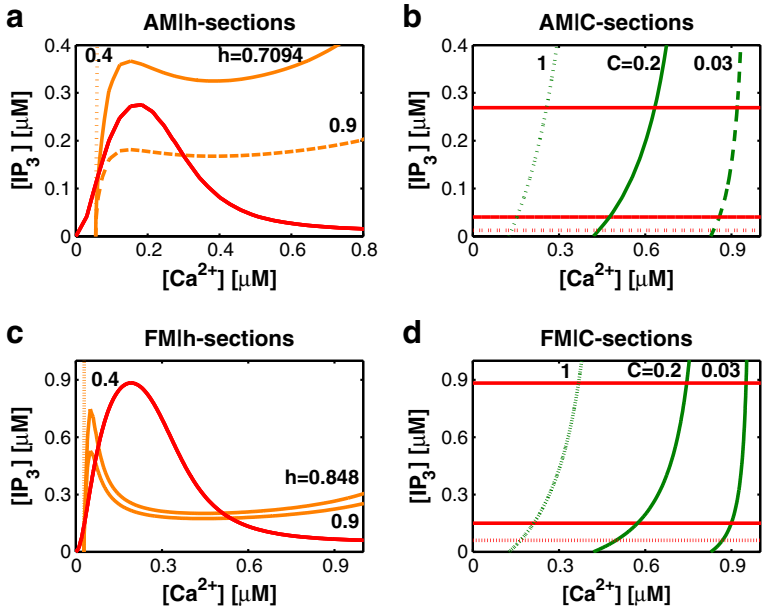

Fig. 8 Projections of the surfaces for $\dot{C} = 0$ (*orange*), $\dot{h} = 0$ (*green*), and $\dot{I} = 0$ (*red*) onto the *I*–*C* plane for different values of **a**, **c** *h* or **b**, **d** *C*, both **a**, **b** in AM and **c**, **d** FM conditions, and allow one to appreciate the nature of coupling between IP_3 metabolism and Ca^{2+} dynamics in the *ChI* model. In particular, since none of the parameters of the equation for IP_3 metabolism (14) are found in the equations for $\dot{C} = 0$ and $\dot{h} = 0$, the latter surfaces are not affected by inclusion of IP_3 dynamics into the L–R core model. It follows that IP_3 dynamics may influence Ca^{2+} dynamics only through modulations of the dynamics of *h*, i.e., Ca^{2+}-mediated deactivation of CICR IP_3R/channels

Glutamate-triggered Ca^{2+} signals in astrocytes are mediated by group I and II mGluRs [74]. Metabotropic GluRs are G-protein coupled receptors associated with the phosphotidylinositol signaling-cascade pathway [75]. Although it is likely that the type of mGluRs expressed by astrocytes depends on the brain region and the stage of development [76], it seems reasonable to assume that such differences are negligible in terms of the associated second-messenger pathways [77, 78].

The G protein associated with astrocyte mGluRs is a heterotrimer constituted by three subunits: α, β, and γ. Glutamate binding to mGluR triggers receptor-catalyzed exchange of GTP from the $G\beta\gamma$ subunits to the $G\alpha$ subunit. The GTP-loaded $G\alpha$ subunit then dissociates from the G protein in the membrane plane and binds to a colocalized PLCβ (Fig. 1a, e). Upon binding to $G\alpha$, the activity of PLCβ substantially increases, thus promoting PIP_2 hydrolysis and IP_3 production. Activation of PLCβ can therefore, to a first approximation, be directly linked to the number of bound mGluRs, and hence to the level of external stimulation. It follows that glutamate-dependent IP_3 production can be written in the following generic form:

$$v_{\mathrm{glu}}(\gamma, C) = \bar{v}_{\beta} \cdot R(\gamma, C) \tag{15}$$

where $\bar{v}_{\beta}$ is the maximal PLCβ rate that depends on the surface density of mGluRs and $R(\gamma,C)$ is the fraction of activated (bound) mGluRs. Experimental evidence shows that PLCβ activity (i.e., $\bar{v}_{\beta}$ in (15)) is also dependent on intracellular Ca^{2+} [49]. Notwithstanding, such dependence seems to occur for $[Ca^{2+}] > 10$ μM, hence out of our physiological range [54]. Therefore, Ca^{2+} dependence of PLCβ maximal rate will not be considered here.

$R(\gamma,C)$ can be expressed in terms of extracellular glutamate concentration (γ) at the astrocytic plasma membrane, assuming a Hill-binding reaction scheme, with an exponent ranging between 0.5 and 1 [60]. In the current study, we choose 0.7, yielding:

$$R(\gamma, C) = \mathrm{Hill}\left(\gamma^{0.7}, K_{\gamma}(\gamma, C)\right). \tag{16}$$

In (16), $R(\gamma,C)$ is expressed as a Hill function with a midpoint that depends on glutamate and intracellular Ca^{2+} concentrations. This choice was motivated by the termination mechanism of PLCβ signaling that occurs essentially through two reaction pathways [48]: (a) reconstitution of the inactive G-protein heterotrimer due to the intrinsic GTPase activity of activated $G\alpha$ subunits and (b) PKC phosphorylation of the receptor, or of the G protein, or of PLCβ, or some combination thereof. We lump both effects into a single term, $K_{\gamma}(\gamma,C)$, such that the effective Hill midpoint of $R(\gamma,C)$ increases as PLCβ termination takes over, namely:

$$K_{\gamma}(\gamma,C) = K_{\mathrm{R}}\left(1 + \frac{K_{\mathrm{p}}}{K_{\mathrm{R}}}\mathrm{Hill}\left(\gamma^{0.7}, K_{\mathrm{R}}\right)\mathrm{Hill}\left(C, K_{\pi}\right)\right). \tag{17}$$

Here, K_{R} is the Hill midpoint of glutamate binding with its receptor whereas K_{p} measures the increment of the apparent affinity of the receptor due to PLCβ terminating signals.

$\mathrm{Hill}(\gamma^{0.7}, K_{\mathrm{R}})$ accounts for the intrinsic GTPase-dependent PLCβ activity termination, as this effect is linked to the fraction of activated $G\alpha$ subunits and therefore can be put in direct proportionality with the fraction of bound receptors. $\mathrm{Hill}(C, K_{\pi})$ instead accounts for PKC-related phosphorylation-dependent termination of PLCβ activity. Experimental data suggest that the target of PKC in this case is either the G protein or PLCβ itself [79]. Generally speaking, phosphorylation by PKC may modulate the efficiency of ligand-binding by the receptors, the coupling of occupied receptors to the G protein, or the coupling of the activated G protein to PLCβ [80]. All these effects indeed are lumped into (17), as explained below.

PKC is activated in a complex fashion (Fig. 1e). Indeed, its activation by mere intracellular Ca^{2+} is minimal [81], while full activation is obtained by binding of the coactivator DAG. In agreement with this description, PKC activation can be approximated by a generic Hill reaction scheme, whereas Ca^{2+}-dependent PKC phosphorylation can be assumed Michaelis–Menten [79] so that $[\text{PKC*}] \propto \text{Hill}\left([\text{DAG}], K'_{\text{DAG}}\right) \cdot \text{Hill}(C, K_\pi)$. Remarkably, [DAG] can itself be related to intracellular Ca^{2+} concentration [82] so that [PKC*] can be rewritten as $[\text{PKC*}] \propto \text{Hill}(C, K_{\text{DAG}}) \cdot \text{Hill}(C, K_\pi)$. Finally, $K_{\text{DAG}} << K_\pi$ [61, 81, 82] so that we can eventually approximate the product of the two Hill functions by that with the highest midpoint (see Appendix 1 for the derivation of this approximation). That yields: $[\text{PKC*}] \propto \text{Hill}(C, K_\pi)$, which accounts for the second Hill function in (17).

To complete the model, it can be shown by numerical analysis of $K_\gamma(\gamma, C)$ (17) that the term related to the GTPase-dependent PLCβ termination pathway, i.e., $\text{Hill}(\gamma^{0.7}, K_{\text{R}})$, can be neglected to a first approximation (Fig. 9). Hence $K_\gamma(\gamma, C)$ can be simplified as $K_\gamma(C)$:

$$K_\gamma(C) \approx K_{\text{R}}\left(1 + \frac{K_{\text{p}}}{K_{\text{R}}}\text{Hill}(C, K_\pi)\right). \tag{18}$$

Using (15), (16), and (18), our final expression for the glutamate-dependent IP_3 production reads:

$$v_{\text{glu}}(\gamma, C) = \bar{v}_\beta \cdot \text{Hill}\left(\gamma^{0.7}, K_{\text{R}}\left(1 + \frac{K_{\text{p}}}{K_{\text{R}}}\text{Hill}(C, K_\pi)\right)\right). \tag{19}$$

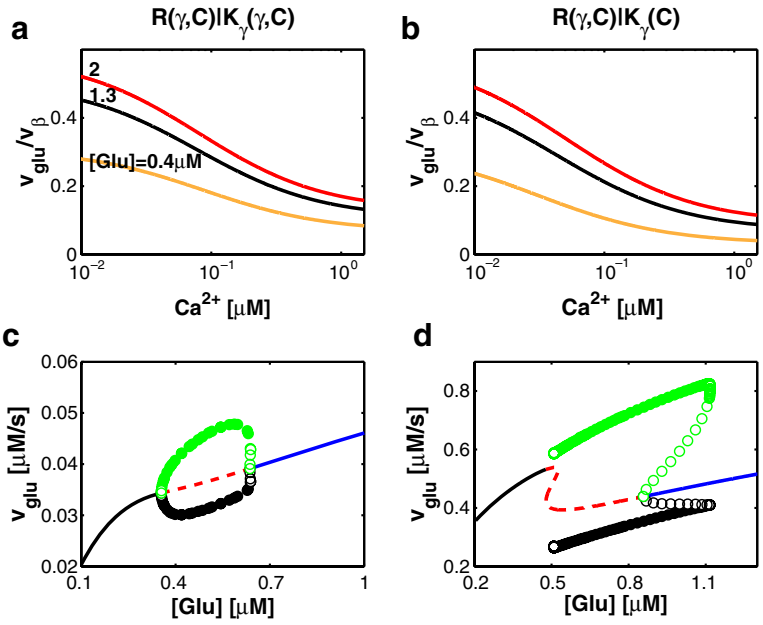

Fig. 9 **a**, **b** Numerical investigation shows that the term related to the GTPase-dependent PLCβ termination pathway in the expression of the agonist-dependent IP_3 production (15 and 17) can be neglected so that $K_\gamma(\gamma, C) \approx K_\gamma(C)$. **c**, **d** Bifurcation behaviors of $v_{\text{glu}}(\gamma, C)$ (19), obtained by substituting γ and C with their values derived from bifurcation diagrams of the agonist-dependent model (see also Figs. 10a and 11a)

Substituting (19) into (14), we obtain

$$\dot{I} = \bar{v}_\beta \cdot \mathrm{Hill}\Big(\gamma^{0.7}, K_\mathrm{R}\left(1 + \tfrac{K_\mathrm{p}}{K_\mathrm{R}}\mathrm{Hill}(C, K_\pi)\right)\Big) + \frac{\bar{v}_\delta}{1 + \frac{I}{\kappa_\delta}}\mathrm{Hill}\big(C^2, K_{\mathrm{PLC}\delta}\big) + \\ -v_{3\mathrm{K}}\mathrm{Hill}\big(C^4, K_\mathrm{D}\big)\,\mathrm{Hill}(I, K_3) - r_{5\mathrm{P}} I\,. \tag{20}$$

This equation, combined with (5) and (6), defines our G-*ChI* model of glutamate-dependent intracellular Ca^{2+} dynamics in astrocytes.

4 Dynamical behaviors and coding modes of the G-*ChI* model

The dynamical features of the G-*ChI* model for different extracellular concentrations of glutamate can be appreciated by inspection of the bifurcation diagrams in Figs. 10 and 11. We note that the choice of $\bar{v}_\beta$, the maximal rate of glutamate-dependent IP_3 production which is linked to the density of receptors on the extracellular side of the astrocyte membrane, can substantially influence the bifurcation structure of the model and the extent of the oscillatory range. Indeed, as $\bar{v}_\beta$ decreases, the oscillatory range expands toward infinite glutamate concentrations, but the amplitude of oscillations concomitantly decreases (at least with regard to the IP_3 concentration).

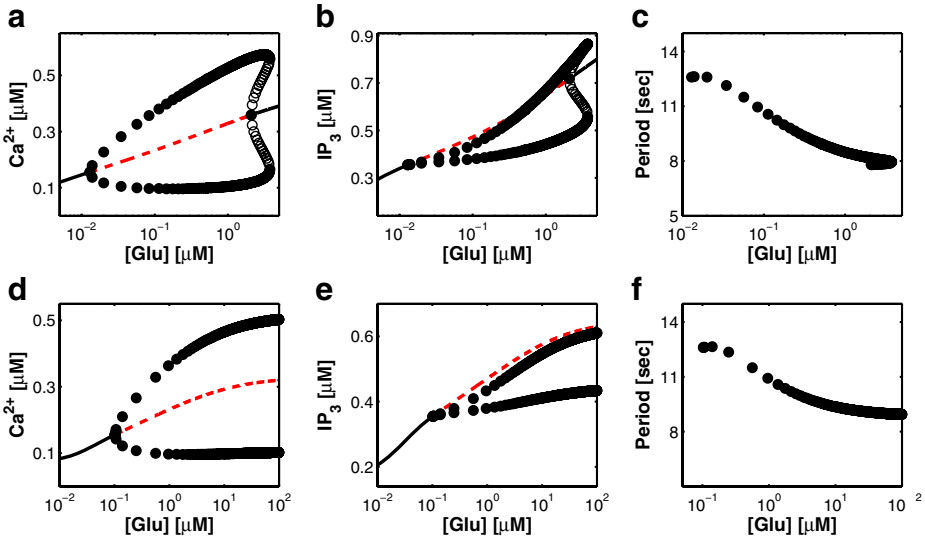

Fig. 10 Bifurcations diagrams for AM-derived parameter sets of the G-*ChI* model (5, 6, 17), show **c**, **f** that the inclusion of IP_3 dynamics remarkably affects the frequency of oscillations. **a**, **d** In particular, Ca^{2+} oscillations are essentially AFM encoding rather than merely AM encoding. **d**–**f** Low values of the glutamate-dependent maximal rate of IP_3 production, $\bar{v}_\beta$, extend the range of oscillations to arbitrarily high glutamate concentrations. In these conditions, phase-locked Ca^{2+}/IP_3 oscillations and pulsations can be observed. Namely, there is a threshold glutamate concentration (which can equivalently be described by a threshold frequency of a pulsed stimulation), for which the frequency of oscillations (pulsations) locks to a particular value and does not change for further elevations of glutamate concentration. Parameters as in Table 1 except for **d**–**f** where $\bar{v}_\beta = 0.05\ \mu\mathrm{M\ s}^{-1}$

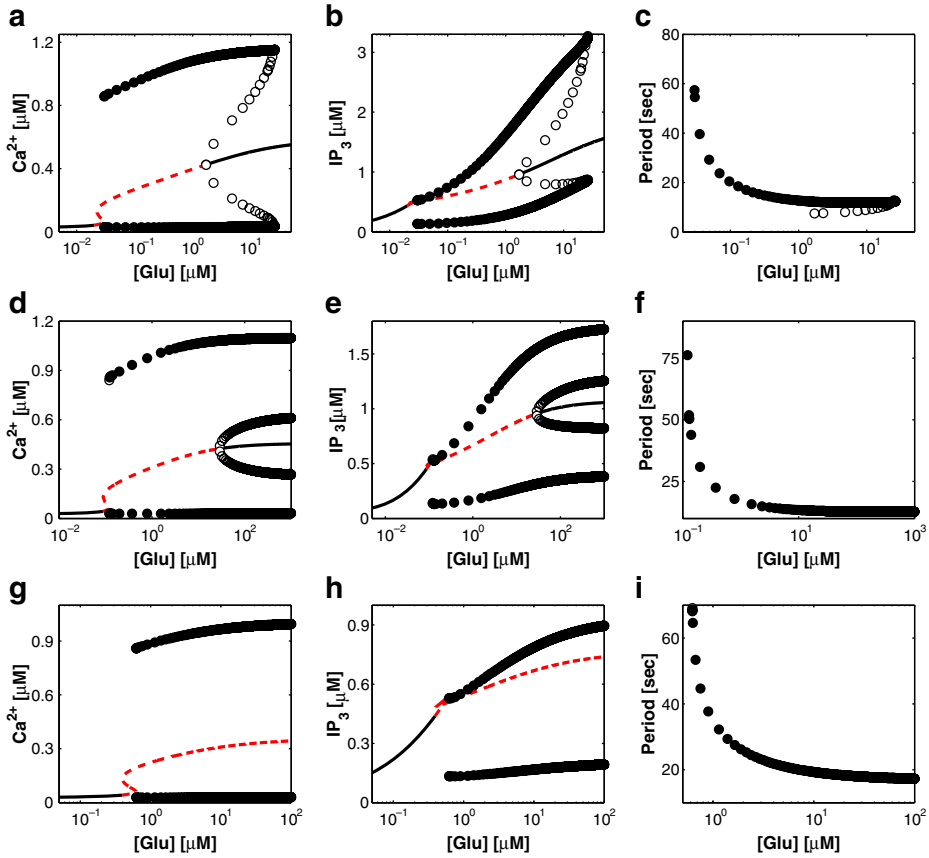

Fig. 11 Bifurcation diagrams of the G-*ChI* model for FM-encoding sets of parameters. **d**–**i** In analogy with Fig. 10, reduced values of $\bar{v}_\beta$, the maximal rate of PLCβ-dependent IP_3 production, extend to infinity the range of oscillations, leading to phase-locking of Ca^{2+}/IP_3 pulsating oscillations. **d**–**f** There is also an intermediate range of $\bar{v}_\beta$ values for which oscillations and fixed concentrations of $[Ca^{2+}]$ and $[IP_3]$ can coexist. **b**, **c**, **e**, **f**, **h**, **i** Unlike Ca^{2+} oscillations, IP_3 oscillations are always AFM encoding with respect to the concentration of agonist (see also Fig. 10b, c, e, f). Parameters as in Table 1 except for **d**–**f** where $\bar{v}_\beta = 0.2\ \mu Ms^{-1}$ and **g**–**i** where $\bar{v}_\beta = 0.05 \mu Ms^{-1}$

The extension of the oscillatory range is due to the shift toward infinity of the subcritical Hopf bifurcation at high glutamate concentrations (compare Fig. 11a, d). Notably, for some values of receptor density, there seems to be coexistence of oscillations and asymptotic stability at high concentrations of extracellular glutamate, depending on the state of the cell prior to the onset of stimulation (Fig. 11d–f).

As $\bar{v}_\beta$ decreases, degradation becomes progressively preponderant so that IP_3 peak levels are lower and the IP_3R channels' open probability is also reduced. Consequently, CICR is weaker and the increase of cytosolic Ca^{2+} is smaller. Then Ca^{2+}-dependent PKC activation is reduced and termination of PLCβ signaling by PKC-dependent phosphorylation is limited. Moreover, if saturation of receptors occurs (i.e., $R(\gamma, C) \approx 1$) and oscillations are observed in this case, it follows that higher extracellular glutamate concentrations cannot further affect the intracellular Ca^{2+} dynamics.

The value of $\bar{v}_\beta$ at which intracellular Ca^{2+} dynamics locks onto stable oscillations also depends on $\bar{v}_\delta$, the strength of the endogen PLCδ-mediated IP_3 production. To some extent, increasing $\bar{v}_\delta$ decreases the minimal $\bar{v}_\beta$ value above which oscillations appear, provided that CICR is strong enough to activate enough PLCδ to keep IP_3 levels above the lower Hopf bifurcation (results not shown).

Coupling between IP_3 and Ca^{2+} dynamics in the G-*ChI* model might have important implications for the encoding of the stimulus. Bifurcation diagrams in Figs. 10 and 11 were derived using different sets of parameters that pertain respectively to AM and FM encoding in the *ChI* model as well as in the L–R core model (see Table 1 and Fig. 3 in Online Supplementary Material). Notwithstanding, the applicability of these definitions to the G-*ChI* model might lead to some ambiguity.

We have previously assumed that AM (FM) encoding exists only if the amplitude (frequency) of oscillations (pulsations) throughout the oscillatory range can at least double with respect to its minimum value [19]. Here, if we consider the AM-derived bifurcation diagrams for Ca^{2+} and IP_3 dynamics (Fig. 10), we note that AM is still found since oscillations occur with arbitrarily small amplitude for the supercritical Hopf point at lower stimulus intensity (Fig. 10a, b, d, e). But the period of oscillations (Fig. 10c, f) at the upper extreme of the oscillatory range is almost half that observed at the onset of oscillations

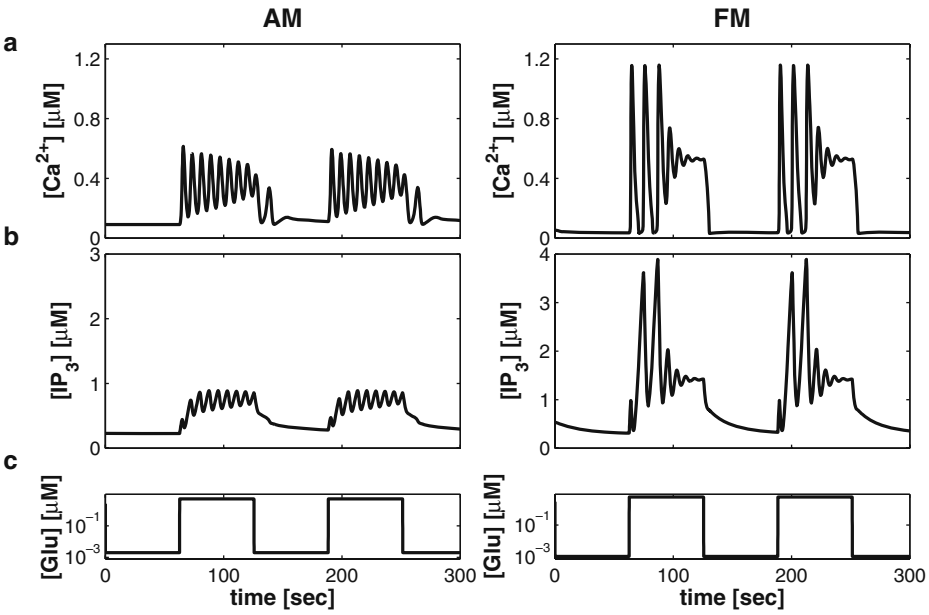

Fig. 12 **a**, **b** Examples of forced burst oscillations exhibited by the G-*ChI* model, under **c** a square-wave stimulus protocol. This figure illustrates how stationary glutamate stimulations are encoded as oscillations and pulsations of the second messengers Ca^{2+} and IP_3. A closer look at oscillatory patterns in **a**, **b** reveals that in our model, IP_3 oscillations always lag Ca^{2+} oscillations. Indeed, the adoption of the L–R core model for CICR at constant IP_3 concentration implies that IP_3 oscillations are not a prerequisite for Ca^{2+} oscillations to occur. Square-wave stimulus: *AM* $\gamma_{\min} = 2$ nM, $\gamma_{\max} = 5$ μM; *FM* $\gamma_{\min} = 1$ nM, $\gamma_{\max} = 6$ μM; *AM*, *FM* duty cycle, 0.5. Note that in the FM case, the value of $\gamma_{\max}$ corresponds in the bifurcation diagrams in Fig. 11a, b to a bistable state (a stable fixed point and a stable limit cycle separated by an unstable limit cycle). This explains why pulsations at high stimulations are of limited duration

at the lower Hopf point. Thus, FM also occurs. Notably, in such conditions, oscillations resemble pulsating dynamics. In other words, rather than pure AM encoding, as we could expect by a set of parameters that provides AM in the *ChI* model (Fig. 1a–c in Online Supplementary Material), it seems that, in the G-*ChI* model, Ca^{2+} oscillations become AFM encoding. Notably, IP_3 dynamics appears to be always AFM encoding both in the AM (Fig. 10b, e) and in the FM-derived bifurcation diagrams (Fig. 11b, f, i).

Conversely, mere FM encoding is essentially preserved for Ca^{2+} dynamics derived from FM encoding sets of parameters in the *ChI* model, although a significant increase of the range of amplitudes of pulsations can be pointed out (compare Fig. 11d with Fig. 3d in Online Supplementary Material). These observations indicate that the G-*ChI* model accounts either for FM or AFM encoding Ca^{2+} oscillations, which are, however always coupled with AFM encoding IP_3 oscillations. In addition, they provide further support to the above-stated notion that IP_3 metabolism could consistently modulate the frequency of Ca^{2+} pulsating dynamics more than their amplitude (see Section 2.3.3).

On the contrary, the amplitude and shape of IP_3 oscillations appear to be dramatically correlated with those of Ca^{2+} oscillations, as a consequence of the numerous Ca^{2+}-dependent feedbacks on IP_3 metabolism. Smooth Ca^{2+} oscillations such as those obtained in AM-like conditions (Fig. 12a, AM) are coupled with small zigzag IP_3 oscillations (Fig. 12b, AM). Under FM conditions instead, pulsating large-amplitude Ca^{2+} variations (Fig. 12a, FM) can be lagged by analogous IP_3 oscillations (Fig. 12b, FM), with the difference that whereas Ca^{2+} pulsations are almost fixed in their amplitude, IP_3 ones can substantially vary.

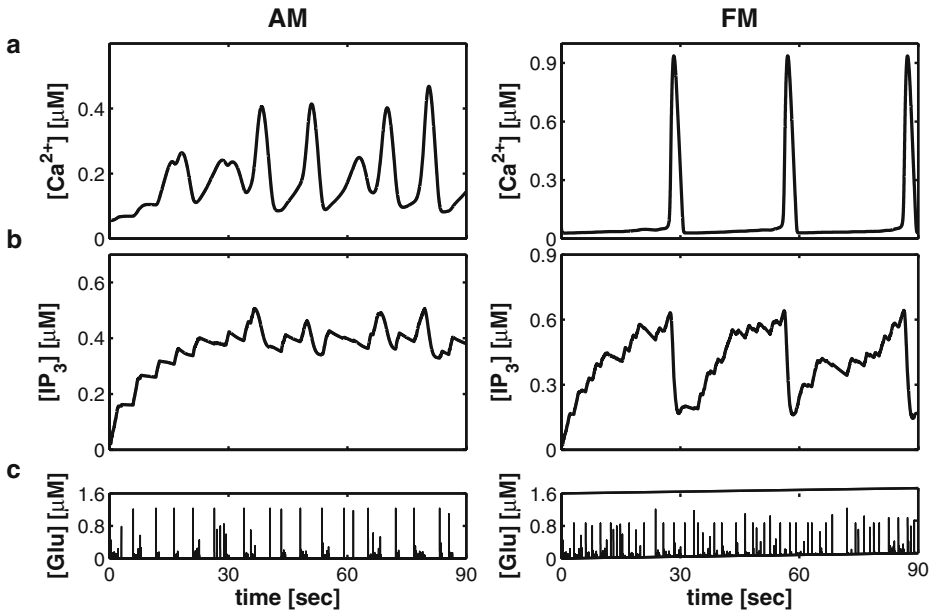

Fig. 13 Simulated Ca^{2+} and IP_3 patterns obtained when the G-*ChI* model is fed with physiologically realistic glutamate stimulations, in the AM and FM case. A striking feature is a remarkable increase of the signal smoothness, when one goes from glutamate stimulus to IP_3 traces (**b**, **c**) and from the latter to Ca^{2+} traces (**a**, **b**). This fact suggests different integrative properties for IP_3 and Ca^{2+}, which are likely to be cross-coupled (see Section 5), with respect to the stimulus

Simulations of physiologically equivalent glutamate stimulation and associated astrocyte Ca^{2+}–IP_3 patterns are shown in Fig. 13. Real multi-array electrode-recording data were considered as inputs of a single glutamatergic synapse (modeled as in Tsodyks and Markram [83]) and a fraction of the released glutamate was assumed to impinge on the astrocyte described by our model. We may notice that, from the stimulus up to Ca^{2+} dynamics, the smoothness of the patterns seems to increase. Indeed, the highly jagged glutamate stimulus turns into a less indented IP_3 signal which is coupled with even smoother Ca^{2+} oscillations. Depending on the inherent cellular properties (Fig. 13, for example, considers two cases associated with different SERCA Ca^{2+} affinities), the difference of smoothness between IP_3 and Ca^{2+} can be dramatic, more likely in the case of FM encoding Ca^{2+} pulsations (compare Fig. 13a–b, AM and FM).

5 Discussion

Calcium dynamics in astrocytes can be driven by extracellular signals (such as the neurotransmitter glutamate) through regulation of the intracellular IP_3 levels. Therefore, a prerequisite for unraveling the response of astrocytes to such signals is a thorough understanding of the complex IP_3-related metabolic pathways that regulate intracellular Ca^{2+} dynamics. Here, we have devised and studied a model for agonist-dependent intracellular Ca^{2+} dynamics that captures the essential biochemical features of the complex regulatory pathways involved in glutamate-induced IP_3 and Ca^{2+} oscillations and pulsations. Our model is simple, yet it retains the essential features of the underlying physiological processes that constitute the intricate IP_3 metabolic network.

More specifically, the equation for IP_3 dynamics is a central component of our model because of the large number of metabolic reactions that it accounts for and because coupling with intracellular Ca^{2+} dynamics is resolved through complex feedback mechanisms. Production of IP_3 depends on the agonist/receptor-dependent PLCβ activation as well as on the endogenous agonist-independent contribution of PLCδ because both isoenzymes are found in astrocytes [48].

We linked the relative expression of these two isoenzymes to the expression of PKC and to the strength of PLCβ regulation by PKC. Indeed, Ca^{2+}-dependent PKC activation can phosphorylate the receptor or PLCβ or a combination thereof, leading to termination of IP_3 production [79]. In astrocytes, this mechanism has been suggested to limit the duration of Ca^{2+} oscillations, thus defining their frequencies [82]. In agreement with this idea, a stronger PKC-dependent inhibition of PLCβ shrank the oscillatory range in our model astrocyte and led to the progressive loss of long-period oscillations.

In our model, the PKC-dependent inhibition of PLCβ is counteracted if PLCδ expression is high enough to support high IP_3 production levels and the resulting release of Ca^{2+} from the intracellular stores. This observation raises the possibility of phase-locked Ca^{2+} oscillations under conditions of intense stimulation. Phase-locked Ca^{2+} oscillations were also found in other models of agonist-dependent intracellular Ca^{2+} dynamics [84–86] and are often associated with pathological conditions [87, 88]. In our model, persistent pulsating Ca^{2+} dynamics that are essentially independent of the level of stimulation are observed for weak maximal rates of IP_3 production by PLCβ (Figs. 10d–e, 11g–h). In astrocytes, such persistent oscillations could also be interpreted as a fingerprint of pathological conditions [1, 89]. In fact, a decay of PLCβ activity is likely to occur, for instance, if the

density of effective metabotropic receptors in the astrocytic plasma membrane decreases, such as in the case of epileptic patients with Ammon's horn sclerosis [90].

We note that, although focusing on stimulus-triggered Ca^{2+} oscillations, our study also hints, at a possible link between modulation of frequency and amplitude of Ca^{2+} pulsations and spontaneous Ca^{2+} dynamics. Recently, it has been shown that the interpulse interval of the spontaneous Ca^{2+} oscillations is inherently stochastic [91, 92]. In particular, experimental observations are compatible with model studies of a local stochastic nucleation mechanism that is amplified by the spatial coupling among IP_3R clusters through Ca^{2+} or IP_3 diffusion [92, 93]. Our analysis may provide meaningful clues to identify what factors and processes within the cell could affect the rate of wave nucleation. More specifically, we may predict that putative intracellular IP_3 dynamics could affect the statistics of Ca^{2+} interpulse intervals not only in terms of spatial coupling among IP_3R clusters by means of intracellular IP_3 gradients but also by modulation of either the recovery from Ca^{2+} inhibition or the progressive sensitization of IP_3Rs by Ca^{2+} [94]. The resulting scenario therefore would still be that of a local stochastic nucleation mechanism amplified by IP_3R spatial coupling, but the local IP_3R and SERCA parameters would vary according to the biochemical regulation system presented in the current work.

A critical question in experiments is the identification of the mechanism that drives IP_3 oscillations and pulsations [57, 95–97]. In our model, self-sustained IP_3 oscillations are brought about by the coupling of IP_3 metabolism with Ca^{2+} dynamics. In other words, our model can be considered as a self-consistent astrocytic generator of Ca^{2+} dynamics. This might have broad implications for astrocyte encoding of information and neuron–glia communication.

We previously demonstrated that modulation by astrocytes of synaptic information transfer could account for some of the peculiar dynamics observed in spontaneous activity of cultured cortical networks [13]. In particular, a simple neuron–glia circuit composed of an autaptic neuron "talking" with a proximal astrocyte could serve as a self-consistent oscillator when fed by weak external signals. The results presented in the current study suggest an alternative, more robust, way (independent of synaptic architecture) to form glia-based self-consistent oscillators. The relative contribution and significance of either the astrocytic or the IP_3-based hypotheses to the spontaneous network activity need to be assessed by future combined experiments and modeling. Meanwhile, the analysis of our present model suggests that, in astrocytes, different second messenger molecules are engaged in an intricate dialogue, likely meaning that those non-neural cells might be crucially important for deciphering some of the enigmas of neural information processing.

Another significant prediction of our model is that IP_3 dynamics is essentially AFM, and Ca^{2+} oscillations/pulsations are inherently FM encoding, that is, they can be either FM or AFM but not AM [18, 19, 98]. In FM, Ca^{2+} oscillations resemble pulses. In contrast, in AFM, their shape is smoother and necessarily depends on the stimulus dynamics.

The assumption that IP_3 oscillations are always AFM encoding could provide an optimal interface between agonist stimuli and intracellular Ca^{2+} signals. The stimuli impinge on the cell in the form of trains of pulses or bursts of pulses and information is carried in the timing of these pulses rather than in their amplitude [99]. AFM features in IP_3 signals could perfectly match these stimuli, embedding the essential features of the spectrum of the signal into the spectrum of the IP_3 transduction. Hence, IP_3 signaling with FM features could offer an efficient way to keep the essence of the information of the stimulus. On the other hand, because Ca^{2+} signals are triggered primarily by sufficiently ample elevations of IP_3 [35],

the coexistence of AM features within the IP_3 signal seems to be a necessary prerequisite in order to trigger CICR.

The fact that coupling of IP_3 metabolism with CICR does not allow pure AM encoding is in general agreement with experimental data on intracellular Ca^{2+} signaling in several cells [100, 101] including astrocytes [3]. Notwithstanding, the possibility of AFM-encoding Ca^{2+} oscillations has recently come up as a reliable alternative mechanism to explain gliotransmitter exocytosis, which is dependent on a specific agonist that triggers astrocyte Ca^{2+} dynamics [21, 102].

The above could be relevant to understanding the origin of the integrative properties of Ca^{2+} signaling in astrocytes [103]. Our analysis in fact shows that such properties could result from at least two steps of integration, one at the transduction of the agonist signal into IP_3 signal and the other at the cross-coupling between the IP_3 and Ca^{2+} signals. Indeed, AFM-encoding IP_3 dynamics could deploy smoothing of the highly indented agonist stimulus, thus hinting at possible integrative properties for IP_3 signals (Fig. 13). On the other hand, the associated Ca^{2+} patterns look even smoother, suggesting a further integration step that likely relies only on the inherent features of CICR.

Acknowledgements The authors wish to thank Vladimir Parpura, Giorgio Carmignoto, and Ilyia Bezprozvanny for insightful conversations. V. V. acknowledges the support of the U.S. National Science Foundation I2CAM International Materials Institute Award, Grant DMR-0645461. This research was supported by the Tauber Family Foundation, by the Maguy-Glass Chair in Physics of Complex Systems at Tel Aviv University, by the NSF-sponsored Center for Theoretical Biological Physics (CTBP), grants PHY-0216576 and 0225630, and by the University of California at San Diego.

Appendix 1

For the sake of simplicity, we have adopted throughout the text the following notation for the generic Hill function:

$$\mathrm{Hill}(x^n, K) \equiv \frac{x^n}{x^n + K^n}$$

where n is the Hill coefficient and K is the midpoint of the Hill function, namely the value of x at which $\mathrm{Hill}\,(x^n, K)|_{x=K} = 1/2$.

It can be shown that the product of two Hill functions can be approximated by the Hill function with the greatest midpoint, when the two midpoints are distant enough from each others, that is:

$$\mathrm{Hill}\,(x^n, K_1) \cdot \mathrm{Hill}(x^n, K_2) \approx \mathrm{Hill}(x^n, K_2)$$

if and only if $K_1 << K_2$ (Fig. 1, Online Supplementary Material). Indeed, under such conditions, $\mathrm{Hill}(x^n, K_1) \cdot \mathrm{Hill}(x^n, K_2) >> 0$ only when $x >> K_1$, hence

$$\begin{aligned}\mathrm{Hill}(x^n, K_1) \cdot \mathrm{Hill}(x^n, K_2) &= \frac{x^{2n}}{x^{2n} + \left(K_1^n + K_2^n\right) x^n + K_1^n K_2^n} \\ &\approx \frac{x^{2n}}{x^{2n} + K_2^n x^n} = \mathrm{Hill}(x^n, K_2)\,.\end{aligned}$$

This result can be extended to the product of N Hill functions, that is:

$$\prod_{i=1}^{N} \text{Hill}(x^n, K_i) \approx \text{Hill}(x^n, \max(K_1, \ldots, K_N))$$

provided that $K_1 << K_2 << \ldots << K_N$.

Notably, the product of Hill function is not the only case in which a functions composed by Hill functions can be approximated by a mere Hill function: other examples are given by functions of the type $\text{Hill}((\text{Hill}(x^n, K_1))^m, K_2)$ or $\text{Hill}(x^m, K_1 \cdot \text{Hill}(x^n, K_2))$ (see Fig. 2 in Online Supplementary Material).

Appendix 2

We seek an expression for [CaMKII*] based on the following kinetic reaction scheme:

$$4\text{Ca}^{2+} + \text{CaM} \underset{k_u}{\overset{k_b}{\rightleftarrows}} \text{CaM}^{+} \tag{21}$$

$$\text{KII} + \text{CaM}^{+} \underset{k_{-1}}{\overset{k_1}{\rightleftarrows}} \text{CaMKII} \underset{k_{-2}}{\overset{k_2}{\rightleftarrows}} \text{CaMKII*}. \tag{22}$$

Let us first consider the reaction chain (22). We can assume that the second step is very rapid with respect to the first one [58, 104] so that generation of CaMKII* is in equilibrium with CaMKII consumption, namely:

$$[\text{CaMKII*}] \approx \frac{k_2}{k_{-2}} [\text{CaMKII}]. \tag{23}$$

Then, under the hypothesis of quasisteady state for CaMKII, we can write:

$$\frac{d}{dt}[\text{CaMKII}] = k_1 [\text{KII}][\text{CaM}^{+}] - (k_{-1} + k_2)[\text{CaMKII}] + k_{-2}[\text{CaMKII*}] \approx 0. \tag{24}$$

It follows that incorporation of (23) into (24) leads to:

$$[\text{CaMKII*}] = K_1 K_2 [\text{KII}][\text{CaM}^{+}] \tag{25}$$

where $K_i = k_i / k_{-i}$. Defining $[\text{KII}]_\text{T} = [\text{KII}] + [\text{CaMKII}] + [\text{CaMKII*}]$ as the total kinase II concentration and assuming it constant, we can rewrite (25) as follows:

$$[\text{CaMKII*}] = \frac{K_2 [\text{KII}]_\text{T}}{1 + K_2} \frac{[\text{CaM}^{+}]}{[\text{CaM}^{+}] + K_m} \tag{26}$$

with $K_m = (K_1 (K_2 + 1))^{-1}$.

The substrate concentration for the enzymatic reaction (22) is provided by reaction (21) according to which:

$$[\text{CaM}^{+}] = [\text{CaM}] \frac{[\text{Ca}^{2+}]^4}{[\text{Ca}^{2+}]^4 + K_\text{d}} \tag{27}$$

with $K_d = k_u/k_b$. Therefore, substituting (27) into (26), we obtain:

$$[\text{CaMKII*}] = \frac{K_2\,[\text{KII}]_T}{1+K_2}\left(1+\frac{K_m}{[\text{CaM}]}\right)^{-1}\frac{[Ca^{2+}]^4}{[Ca^{2+}]^4+\frac{K_m K_d}{K_m+[\text{CaM}]}} \tag{28}$$

so that $[\text{CaMKII*}] \propto \text{Hill}\left([Ca^{2+}]^4, K_D\right)$ with $K_D = \left(\frac{K_m K_d}{K_m+[\text{CaM}]}\right)^{1/4}$.

References

1. Volterra, A., Meldolesi, J.: Astrocytes, from brain glue to communication elements: the revolution continues. Nat. Rev., Neurosci. **6**(8), 626–640 (2005). doi:10.1038/nrn1722
2. Wang, X., Lou, N., Xu, Q., Tian, G.F., Peng, W.G., Han, X., Kang, J., Takano, T., Nedergaard, M.: Astrocytic Ca^{2+} signaling evoked by sensory stimulation *in vivo*. Nat. Neurosci. **9**(6), 816–823 (2006). doi:10.1038/nn1703
3. Pasti, L., Volterra, A., Pozzan, T., Carmignoto, G.: Intracellular calcium oscillations in astrocytes: a highly plastic, bidirectional form of communication between neurons and astrocytes *in situ*. J. Neurosci. **17**(20), 7817–7830 (1997)
4. Porter, J.T., McCarthy, K.D.: Hippocampal astrocytes in situ respond to glutamate released from synaptic terminals. J. Neurosci. **16**(16), 5073–5081 (1996)
5. Parpura, V., Basarsky, T.A., Liu, F., Jeftinija, K., Jeftinija, S., Haydon, P.G.: Glutamate-mediated astrocyte–neuron signalling. Nature **369**, 744–747 (1994). doi:10.1038/369744a0
6. Dani, J.W., Chernjavsky, A., Smith, S.J.: Neuronal activity triggers calcium waves in hippocampal astrocyte networks. Neuron **8**, 429–440 (1992). doi:10.1016/0896-6273(92)90271-E
7. Nett, W.J., Oloff, S.H., McCarthy, K.D.: Hippocampal astrocytes in situ exhibit calcium oscillations that occur independent of neuronal activity. J. Neurophysiol. **87**, 528–537 (2002)
8. Zonta, M., Carmignoto, G.: Calcium oscillations encoding neuron-to-astrocyte communication. J. Physiol. (Paris) **96**, 193–198 (2002). doi:10.1016/S0928-4257(02)00006-2
9. Stout, C.E., Costantin, J.L., Naus, C.C.G., Charles, A.C.: Intercellular calcium signaling in astrocytes via ATP release through connexin hemichannels. J. Biol. Chem. **277**(12), 10482–10488 (2002). doi:10.1074/jbc.M109902200
10. Charles, A.: Intercellular calcium waves in glia. Glia **24**(1), 39–49 (1998). doi:10.1002/(SICI)1098-1136(199809)24:1<39::AID-GLIA5>3.0.CO;2-W
11. Cornell-Bell, A.H., Finkbeiner, S.M., Cooper, M.S., Smith, S.J.: Glutamate induces calcium waves in cultured astrocytes: long-range glial signaling. Science **247**(4941), 470–473 (1990). doi:10.1126/science.1967852
12. Evanko, D.S., Sul, J.Y., Zhang, Q., Haydon, P.G.: The regulated release of transmitters from astrocytes. In: Hatton, G.I., Parpura, V. (eds.) Glial–neuronal Signaling, pp. 397–416. Kluwer Academic, New York (2004)
13. Volman, V., Ben-Jacob, E., Levine, H.: The astrocyte as a gatekeeper of synaptic information transfer. Neural Comput. **19**, 303–326 (2007). doi:10.1162/neco.2007.19.2.303
14. Fellin, T., Pascual, O., Gobbo, S., Pozzan, T., Haydon, P.G., Carmignoto, G.: Neuronal synchrony mediated by astrocytic glutamate through activation of extrasynaptic NMDA receptors. Neuron **43**, 729–743 (2004). doi:10.1016/j.neuron.2004.08.011
15. Araque, A., Parpura, V., Sanzgiri, R.P., Haydon, P.G.: Glutamate-dependent astrocyte modulation of synaptic transmission between cultured hippocampal neurons. Eur. J. Neurosci. **10**, 2129–2142 (1998). doi:10.1046/j.1460-9568.1998.00221.x
16. Fellin, T., Carmignoto, G.: Neurone-to-astrocyte signalling in the brain represents a distinct multifunctional unit. J. Physiol. **559**(1), 3–15 (2004). doi:10.1113/jphysiol.2004.063214
17. Bernardinelli, Y., Magistretti, P.J., Chatton, J.Y.: Astrocytes generate Na^+-mediated metabolic waves. Proc. Natl. Acad. Sci. U.S.A. **101**(41), 14937–14942 (2004). doi:10.1073/pnas.0405315101
18. De Pittà, M., Volman, V., Levine, H., Pioggia, G., De Rossi, D., Ben-Jacob, E.: Coexistence of amplitude and frequency modulations in intracellular calcium dynamics. Phys. Rev. E **77**(3), 030903(R) (2008)
19. De Pittà, M., Volman, V., Levine, H., Ben-Jacob, E.: Multimodal encoding in a simplified model of intracellular calcium signaling. Cogn. Proc. **10**(Suppl 1), S55–S70 (2008). doi:10.1007/s10339-008-0242-y

20. Parpura, V.: Glutamate-mediated bi-directional signaling between neurons and astrocytes. In: Hatton, G.I., Parpura, V. (eds.) Glial–neuronal Signaling, pp. 365–396. Kluwer Academic, Boston, MA (2004)
21. Carmignoto, G.: Reciprocal communication systems between astrocytes and neurones. Prog. Neurobiol. **62**, 561–581 (2000). doi:10.1016/S0301-0082(00)00029-0
22. Finkbeiner, S.M.: Glial calcium. Glia **9**, 83–104 (1993). doi:10.1002/glia.440090202
23. Perea, G., Araque, A.: Synaptic regulation of the astrocyte calcium signal. J. Neural Transm. **112**, 127–135 (2005b). doi:10.1007/s00702-004-0170-7
24. Li, Y., Rinzel, J.: Equations for $InsP_3$ receptor-mediated $[Ca^{2+}]_i$ oscillations derived from a detailed kinetic model: a Hodgkin–Huxley like formalism. J. Theor. Biol. **166**, 461–473 (1994). doi:10.1006/jtbi.1994.1041
25. Kazantsev, V.B.: Spontaneous calcium signals induced by gap junctions in a network model of astrocytes. Phys. Rev. E **79**(1), 010901 (2009). doi:10.1103/PhysRevE.79.010901
26. Politi, A., Gaspers, L.D., Thomas, A.P., Höfer, T.: Models of IP_3 and Ca^{2+} oscillations: frequency encoding and identification of underlying feedbacks. Biophys. J. **90**, 3120–3133 (2006). doi:10.1529/biophysj.105.072249
27. Höfer, T., Venance, L., Giaume, C.: Control and plasticity of intercellular calcium waves in astrocytes: a modeling approach. J. Neurosci. **22**(12), 4850–4859 (2002)
28. Sneyd, J., Wetton, B.T.R., Charles, A.C., Sanderson, M.J.: Intercellular calcium waves mediated by diffusion of inositol trisphosphate: a two-dimensional model. Am. J. Physiol. **268**(37), C1537–C1545 (1995)
29. Dupont, G., Goldbeter, A.: One-pool model for Ca^{2+} oscillations involving Ca^{2+} and inositol 1,4,5-trisphosphate as co-agonists for Ca^{2+} release. Cell Calcium **14**, 311–322 (1993). doi:10.1016/0143-4160(93)90052-8
30. Meyer, T., Stryer, L.: Molecular model for receptor-stimulated calcium spiking. Proc. Natl. Acad. Sci. U.S.A. **85**, 5051–5055 (1988). doi:10.1073/pnas.85.14.5051
31. Falcke, M.: Reading the patterns in living cells—the physics of Ca^{2+} signaling. Adv. Phys. **53**(3), 255–440 (2004). doi:10.1080/00018730410001703159
32. Communi, D., Gevaert, K., Demol, H., Vandekerckhove, J., Erneux, C.: A novel receptor-mediated regulation mechanism of type I inositol polyphosphate 5-phosphatase by calcium/calmodulin-dependent protein kinase II phosphorylation. J. Biol. Chem. **276**(42), 38738–38747 (2001). doi:10.1074/jbc.M105640200
33. Berridge, M.J., Lipp, P., Bootman, M.D.: The versatility and universality of calcium signalling. Nat. Rev. Mol. Cell Biol. **1**, 11–21 (2000). doi:10.1038/35036035
34. Agulhon, C., Petravicz, J., McMullen, A.B., Sweger, E.J., Minton, S.K., Taves, S.R., Casper, K.B., Fiacco, T.A., McCarthy, K.D.: What is the role of astrocyte calcium in neurophysiology? Neuron **59**, 932–946 (2008). doi:10.1016/j.neuron.2008.09.004
35. Li, Y.X., Rinzel, J., Keizer, J., Stojilkovič, S.S.: Calcium oscillations in pituitary gonadotrophs: comparison of experiment and theory. Proc. Natl. Acad. Sci. U.S.A. **91**, 58–62 (1994). doi:10.1073/pnas.91.1.58
36. De Young, G.W., Keizer, J.: A single-pool inositol 1,4,5-trisphosphate-receptor-based model for agonist-stimulated oscillations in Ca^{2+} concentration. Proc. Natl. Acad. Sci. U.S.A. **89**, 9895–9899 (1992)
37. Berridge, M.J.: Inositol trisphosphate and calcium signalling. Nature **361**, 315–323 (1993). doi:10.1038/361315a0
38. Bezprozvanny, I., Watras, J., Ehrlich, B.E.: Bell-shaped calcium-response curves of $Ins(1,4,5)P_3$- and calcium-gated channels from endoplasmic reticulum of cerebellum. Nature **351**, 751–754 (1991). doi:10.1038/351751a0
39. Iino, M.: Biphasic Ca^{2+}-dependence of inositol 1,4,5-trisphosphate-induced Ca^{2+} release in smooth muscle cells of the guinea pig Taenia caeci. J. Gen. Physiol. **95**, 1103–1112 (1990). doi:10.1085/jgp.95.6.1103
40. Lytton, J., Westlin, M., Burk, S.E., Shull, G.W., MacLennan, D.H.: Functional comparisons between isoforms of the sarcoplasmic or endoplasmic reticulum of calcium pumps. J. Biol. Chem. **267**(20), 14483–14489 (1992)
41. Keizer, J., Li, Y., Stojilkovič, S., Rinzel, J.: $InsP_3$-induced Ca^{2+} excitability of the endoplasmic reticulum. Mol. Biol. Cell **6**, 945–951 (1995)
42. Carafoli, E.: Calcium signaling: a tale for all seasons. Proc. Natl. Acad. Sci. U.S.A. **99**(3), 1115–1122 (2002). doi:10.1073/pnas.032427999
43. Foskett, J.K., Roifman, C.M., Wong, D.: Activation of calcium oscillations by thapsigargin in parotid acinar cells. J. Biol. Chem. **266**(5), 2778–2782 (1991)

44. Rooney, T.A., Renard, D.C., Sass, E.J., Thomas, A.P.: Oscillatory cytosolic calcium waves independent of stimulated inositol 1,4,5-trisphosphate formation in hepatocytes. J. Biol. Chem. **266**(19), 12272–12282 (1991)
45. Jaffe, L.F.: Classes and mechanisms of calcium waves. Cell Calcium **14**, 736–745 (1993). doi:10.1016/0143-4160(93)90099-R
46. Berridge, M.J.: Calcium oscillations. J. Biol. Chem. **265**(17), 9583–9586 (1990)
47. Verkhratsky, A., Kettenmann, H.: Calcium signaling in glial cells. Trends Neurosci. **19**, 346–352 (1996). doi:10.1016/0166-2236(96)10048-5
48. Rebecchi, M.J., Pentyala, S.N.: Structure, function, and control of phosphoinositide-specific phospholipase C. Physiol. Rev. **80**(4), 1291–1335 (2000)
49. Rhee, S.G., Bae, Y.S.: Regulation of phosphoinositide-specific phospholipase C isozymes. J. Biol. Chem. **272**, 15045–15048 (1997). doi:10.1074/jbc.272.24.15045
50. Rhee, S.G.: Regulation of phosphoinositide-specific phospholipase C. Annu. Rev. Biochem. **70**, 281–312 (2001). doi:10.1146/annurev.biochem.70.1.281
51. Essen, L., Perisic, O., Lynch, D.E., Katan, M., Williams, R.L.: A ternary metal binding site in the C2 domain of phosphoinositide-specific phospholipase C-δ1. Biochemistry **37**(10), 4568–4680 (1997)
52. Essen, L., Perisic, O., Cheung, R., Katan, M., Williams, R.L.: Crystal structure of a mammalian phosphoinositide-specific phospholipase C. Nature **380**, 595–602 (1996). doi:10.1038/380595a0
53. Pawelczyk, T., Matecki, A.: Structural requirements of phospholipase C δ1 for regulation by spermine, sphingosine and sphingomyelin. Eur. J. Biochem. **248**, 459–465 (1997). doi:10.1111/j.1432-1033.1997.00459.x
54. Allen, V., Swigart, P., Cheung, R., Cockcroft, S., Katan, M.: Regulation of inositol-specific phospholipase Cδ by changes in Ca^{2+} ion concentrations. Biochem. J. **327**, 545–552 (1997)
55. Stryer, L.: Biochemistry, 4th edn. Freeman, New York (1999)
56. Irvine, R.F., Letcher, A.J., Heslop, J.P., Berridge, M.J.: The inositol tris/tetrakisphosphate pathway—demonstration of Ins(1,4,5)P_3 3-kinase activity in animal tissues. Nature **320**, 631–634 (1986). doi:10.1038/320631a0
57. Sims, C.E., Allbritton, N.L.: Metabolism of inositol 1,4,5-triphosphate and inositol 1,3,4,5-tetrakisphosphate by the oocytes of *Xenopus laevis*. J. Biol. Chem. **273**(7), 4052–4058 (1998)
58. De Konick, P., Schulman, H.: Sensitivity of CaM kinase II to the frequency of Ca^{2+} oscillations. Science **279**, 227–230 (1998). doi:10.1126/science.279.5348.227
59. Takazawa, K., Passareiro, H., Dumont, J.E., Erneux, C.: Purification of bovine brain inositol 1,4,5-trisphosphate 3-kinase. Identification of the enzyme by sodium dodecyl sulfate/polyacrylamide-gel electrophoresis. Biochem. J. **261**, 483–488 (1989)
60. Suzuki, Y., Moriyoshi, E., Tsuchiya, D., Jingami, H.: Negative cooperativity of glutamate binding in the dimeric metabotropic glutamate receptor subtype I. J. Biol. Chem. **279**(34), 35526–35534 (2004). doi:10.1074/jbc.M404831200
61. Shinomura, T., Asaoka, Y., Oka, M., Yoshida, K., Nishizuka, Y.: Synergistic action of diacylglycerol and unsaturated fatty acid for protein kinase C activation: its possible implications. Proc. Natl. Acad. Sci. U.S.A. **88**, 5149–5153 (1991). doi:10.1073/pnas.88.12.5149
62. Kawabata, S., Tsutumi, R., Kohara, A., Yamaguchi, T., Nakanishi, S., Okada, M.: Control of calcium oscillations by phosphorylation of metabotropic glutamate receptors. Nature **383**, 89–92 (1996). doi:10.1038/383089a0
63. Zhang, B.X., Zhao, H., Muallem, S.: Calcium dependent kinase and phosphatase control inositol-1,4,5-trisphopshate-mediated calcium release: modification by agonist stimulation. J. Biol. Chem. **268**(5), 10997–11001 (1993)
64. Dupont, G., Erneux, C.: Simulations of the effects of inositol 1,4,5-trisphosphate 3-kinase and 5-phosphatase activities on Ca^{2+} oscillations. Cell Calcium **22**(5), 321–331 (1997). doi:10.1016/S0143-4160(97)90017-8
65. Togashi, S., Takazawa, K., Endo, T., Erneux, C., Onaya, T.: Structural identification of the *myo*-inositol 1,4,5-trisphosphate-binding domain in rat brain inositol 1,4,5-trisphopshate 3-kinase. Biochem. J. **326**, 221–225 (1997)
66. Verjans, B., Lecocq, R., Moreau, C., Erneux, C.: Purification of bovine brain inositol-1,4,5-trisphosphate 5-phosphatase. Eur. J. Biochem. **204**, 1083–1087 (1992). doi:10.1111/j.1432-1033.1992.tb16732.x
67. Communi, D., Vanweyenberg, V., Erneux, C.: D-*myo*-inositol 1,4,5-trisphosphate 3-kinase A is activated by receptor activation through a calcium: calmodulin-dependent protein kinase II phosphorylation mechanism. EMBO J. **16**(8), 1943–1952 (1997). doi:10.1093/emboj/16.8.1943
68. Sim, S.S., Kim, J.W., Rhee, S.G.: Regulation of D-*myo*-inositol 1,4,5-trisphosphate 3-kinase by cAMP-dependent protein kinase and protein kinase C. J. Biol. Chem. **265**, 10367–10372 (1990)

69. Communi, D., Vanweyenberg, V., Erneux, C.: Molecular study and regulation of D-*myo*-inositol 1,4,5-trisphopshate 3-kinase. Cell. Signal. **7**(7), 643–650 (1995). doi:10.1016/0898-6568(95)00035-N
70. Communi, D., Dewaste, V., Erneux, C.: Calcium-calmodulin-dependent protein kinase II and protein kinase C-mediated phosphorylation and activation of D-*myo*-inositol 1,4,5-trisphosphate 3-kinase B in astrocytes. J. Biol. Chem. **274**, 14734–14742 (1999). doi:10.1074/jbc.274.21.14734
71. Kolodziej, S.J., Hudmon, A., Waxham, M.N., Stoops, J.K.: Three-dimensional reconstructions of calcium/calmodulin-dependent (CaM) kinase IIα and truncated CaM kinase IIα reveal a unique organization for its structural core and functional domains. J. Biol. Chem. **275**(19), 14354–14359 (2000). doi:10.1074/jbc.275.19.14354
72. Hanson, P.I., Meyer, T., Stryer, L., Schulman, H.: Dual role of calmodulin in autophosphorylation of multifunctional CaM kinase may underlie decoding of calcium signals. Neuron **12**, 943–956 (1994). doi:10.1016/0896-6273(94)90306-9
73. Mishra, J., Bhalla, U.S.: Simulations of inositol phosphate metabolism and its interaction with $\mathrm{InsP_3}$-mediated calcium release. Biophys. J. **83**, 1298–1316 (2002)
74. Zur Nieden, R., Deitmer, J.W.: The role of metabotropic glutamate receptors for the generation of calcium oscillations in rat hippocampal astrocytes *in situ*. Cereb. Cortex **16**, 676–687 (2006). doi:10.1093/cercor/bhj013
75. Teichberg, V.I.: Glial glutamate receptors: likely actors in brain signaling. FASEB J. **5**, 3086–3091 (1991)
76. Gallo, V., Ghiani, A.: Glutamate receptors in glia: new cells, new inputs and new functions. Trends Pharmacol. Sci. **21**, 252–258 (2000). doi:10.1016/S0165-6147(00)01494-2
77. Abe, T., Sugihara, H., Nawa, H., Shigemotoy, R., Mizunoll, N., Nakanishi, S.: Molecular characterization of a novel metabotropic glutamate receptor mGluR5 coupled to inositol phosphate/Ca^{2+} signal transduction. J. Biol. Chem. **267**(19), 13361–13368 (1992)
78. Masu, M., Tanabe, Y., Tsuchida, K., Shigemoto, R., Nakanishi, S.: Sequence and expression of a metabotropic glutamate receptor. Nature **349**, 760–765 (1991). doi:10.1038/349760a0
79. Ryu, S.H., Kin, U., Wahl, M.I., Brown, A.B., Carpenter, G., Huang, K., Rhee, S.G.: Feedback regulation of phospholipase C-β by protein kinase C. J. Biol. Chem. **265**(29), 17941–17945 (1990)
80. Fisher, S.K.: Homologous and heterologous regulation of receptor stimulated phosphoinositide hydrolysis. Eur. J. Pharmacol. **288**, 231–250 (1995). doi:10.1016/0922-4106(95)90035-7
81. Nishizuka, Y.: Protein kinase C and lipid signaling for sustained cellular responses. FASEB J. **9**, 484–496 (1995)
82. Codazzi, F., Teruel, M.N., Meyer, T.: Control of astrocyte Ca^{2+} oscillations and waves by oscillating translocation and activation of protein kinase C. Curr. Biol. **11**(14), 1089–1097 (2001). doi:10.1016/S0960-9822(01)00326-8
83. Tsodyks, M.V., Markram, H.: The neural code between neocortical pyramidal neurons depends on neurotransmitter release probability. Proc. Natl. Acad. Sci. U.S.A. **94**, 719–723 (1997). doi:10.1073/pnas.94.2.719
84. Chay, T., Fan, Y.S., Lee, S.Y.: Bursting, spiking, chaos, fractals and universality in biological rhythms. Int. J. Bifurcat. Chaos **5**, 595–635 (1995). doi:10.1142/S0218127495000491
85. Chay, T., Lee, Y.S., Fan, Y.S.: Appearance of phase-locked Wenckebach-like rhythms, devil's staircase and universality in intracellular calcium spikes in non-excitable cell models. J. Theor. Biol. **174**, 21–44 (1995). doi:10.1006/jtbi.1995.0077
86. Cuthbertson, K.S.R., Chay, T.R.: Modelling receptor-controlled intracellular calcium oscillators. Cell Calcium **12**, 97–108 (1991). doi:10.1016/0143-4160(91)90012-4
87. Uhlhaas, P.J., Singer, W.: Neural synchrony in brain disorders: relevance for cognitive dysfunctions and pathophysiology. Neuron **52**, 155–168 (2006). doi:10.1016/j.neuron.2006.09.020
88. Shrier, A., Dubarsky, H., Rosengarten, M., Guevara, M.R., Nattel, S., Glass, L.: Prediction of complex atrioventricular conduction rhythms in humans with use of the atrioventricular nodal recovery curve. Circulation **76**, 1196–1205 (1987)
89. Balázsi, G., Cornell-Bell, A.H., Moss, F.: Increased phase synchronization of spontaneous calcium oscillations in epileptic human versus normal rat astrocyte cultures. Chaos **13**(2), 515–518 (2003). doi:10.1063/1.1567652
90. Seifert, G., Huttmann, K., Schramm, J., Steinhauser, C.: Enhanced relative expression of glutamate receptor 1 flip AMPA receptor subunits in hippocampal astrocytes of epilepsy patients with Ammon's horn sclerosis. J. Neurosci. **24**, 1996–2003 (2004). doi:10.1523/JNEUROSCI.3904-03.2004
91. Skupin, A., Falcke, M.: Statistical properties and information content of calcium oscillations. Genome Inf. **18**, 44–53 (2008)

92. Skupin, A., Kettenmann, H., Winkler, U., Wartenberg, M., Sauer, H., Tovey, S.C., Taylor, C.W., Falcke, M.: How does intracellular Ca^{2+} oscillate: by chance or by clock? Biophys. J. **94**, 2404–2411 (2008). doi:10.1529/biophysj.107.119495
93. Falcke, M.: On the role of stochastic channel behavior in intracellular Ca^{2+} dynamics. Biophys. J. **84**, 42–56 (2003). doi:10.1016/S0006-3495(03)74831-0
94. Tang, Y., Othmer, H.G.: Frequency encoding in excitable systems with applications to calcium oscillations. Proc. Natl. Acad. Sci. U.S.A. **92**, 7869–7873 (1995). doi:10.1073/pnas.92.17.7869
95. Young, K.W., Nash, M.S., Challiss, J.R.A., Nahorski, S.R.: Role of Ca^{2+} feedback on single cell inositol 1,4,5-trisphosphate oscillations mediated by G-protein-coupled receptors. J. Biol. Chem. **278**, 20753–20760 (2003). doi:10.1074/jbc.M211555200
96. Nash, M.S., Young, K.W., Challiss, J.R.A., Nahorski, S.R.: Intracellular signalling receptor-specific messenger oscillations. Nature **413**, 381–382 (2001). doi:10.1038/35096643
97. Hirose, K., Kadowaki, S., Tanabe, M., Takeshima, H., Lino, M.: Spatiotemporal dynamics of inositol 1,4,5-trisphosphate that underlies complex Ca^{2+} mobilization. Science **284**, 1527–1530 (1999). doi:10.1126/science.284.5419.1527
98. Berridge, M.J.: The AM and FM of calcium signaling. Nature **389**, 759–760 (1997). doi:10.1038/386759a0
99. Sejnowski, T.J., Paulsen, O.: Network oscillations: emerging computational principles. J. Neurosci. **26**(6), 1673–1676 (2006). doi:10.1523/JNEUROSCI.3737-05d.2006
100. Berridge, M.J., Bootman, M.D., Lipp, P.: Calcium—a life and death signal. Nature **395**, 645–648 (1998). doi:10.1038/27094
101. Woods, N.M., Cuthbertson, K.S.R., Cobbold, P.H.: Repetitive transient rises in cytoplasmic free calcium in hormone-stimulated hepatocytes. Nature **319**, 600–602 (1986). doi:10.1038/319600a0
102. Montana, V., Malarkey, E.B., Verderio, C., Matteoli, M., Parpura, V.: Vesicular transmitter release from astrocytes. Glia **54**, 700–715 (2006). doi:10.1002/glia.20367
103. Perea, G., Araque, A.: Properties of synaptically evoked astrocyte calcium signal reveal synaptic information processing by astrocytes. J. Neurosci. **25**(9), 2192–2203 (2005). doi:10.1523/JNEUROSCI.3965-04.2005
104. Thiel, G., Czernik, A.J., Gorelick, F., Nairn, A.C., Greengard, P.: Ca^{2+}/calmodulin-dependent protein kinase II: identification of threonine-286 as the autophosphorylation site in the α subunit associated with the generation of Ca^{2+}-independent activity. Proc. Natl. Acad. Sci. U.S.A. **85**, 6337–6341 (1988). doi:10.1073/pnas.85.17.6337